universität wien

MASTERARBEIT / MASTER'S THESIS

Titel der Masterarbeit / Title of the Master's Thesis

„Effects of Naltrexone on Resting-State Functional Connectivity"

verfasst von / submitted by
Pablo Reinhardt, BSc

angestrebter akademischer Grad / in partial fulfilment of the requirements for the degree of
Master of Science (MSc)

Wien, 2019 / Vienna 2019

Studienkennzahl lt. Studienblatt / degree programme code as it appears on the student record sheet:	A 066 840
Studienrichtung lt. Studienblatt / degree programme as it appears on the student record sheet:	Masterstudium Psychologie UG2002
Betreut von / Supervisor:	Univ.-Prof. Mag. Dr. Claus Lamm
Mitbetreut von / Co-Supervisor:	Mag. Dr. Markus Rütgen

INTRODUCTION

Application of Graph Theory to Resting-State Functional Connectivity

Fascinatingly, the human brain is composed as a genuinely complex network (Sporns, Chialvo, Kaiser & Hilgetag, 2004), comprising a staggering number of approximately 86 billion neurons (Azevedo et al., 2009). These basic neuronal entities form structural and functional networks on spatially and temporally varying scales, allowing for rapid and dynamic, yet resilient information flow (Sporns et al., 2004). To empirically encompass this intrinsically complex network system and derive meaningful conclusions about it, a framework is required which can reliably capture large-scale network properties.

A suchlike framework is provided by graph theory, a mathematical account allowing for the study of the topological organization of networks of various kinds (Braun et al., 2018). Graph theory has been successfully deployed in a considerable bredth of fields which are confronted with complex systems, ranging from, among others, cancer detection in precision oncology (Zhang, Chien, Yong, & Kuang, 2017) to modelling molecule structure in chemistry (Janezic, Milicevic, Nikolic, & Trinajstic, 2015) and, finally, to a wide array of problems within the realms of the neurosciences (Bullmore & Sporns, 2009).

In graph theory, a graph consists of nodes and edges connecting nodes (Bullmore & Sporns, 2009). Depending on the nature of the respective network, nodes can be represented by, for example, interactions between proteins on a cellular level or by individuals in social systems (Bullmore & Sporns, 2012). Graph measures reveal aspects of how a network or graph is connected: these properties allow for inferences about the resilience of a network against disruption, its overall connectedness or its randomness.

Despite obvious differences of various networks on a microscopic level, networks of different kinds share distinct topological properties (Bullmore & Sporns, 2009). In the neurosciences, these properties can be used to infer connectivity markers in clinical and healthy populations alike. Advances in the neurosciences have allowed to deploy graph theory as a powerful method to gain a deeper understanding of functional connectivity (Drakesmith et al., 2015). In this framework, a graph is comprised of anatomically or functionally defined nodes in the brain. Anatomical connectivity relates to structural synaptic edges from varying spatial scale, connecting neuronal units at a given time (Sporns et al., 2004). Functional connectivity explores statistical time-series dependencies between often spatially remote regions of interest by measuring their correlation, covariance or other measures of statistical interrelation (Sporns et al., 2004).

A commonly applied method in studying graph theoretical properties of brain connectivity is resting state functional connectivity (rs-fcMRI), which measures spontaneous blood oxygen level dependent (BOLD) signal fluctuations in participants at rest (Power et al., 2011). For its ability to obtain measures of neural activity of remote brain loci (Power et al., 2011), rs-fcMRI has gained substantial momentum and has since contributed to the discovery of a range of functional networks engaged in a variety of tasks such as the dorsal attention network (DAN) or the default mode network (DMN) (Fox et al., 2005). The DMN is a network which is particularly active at rest (Raichle, 2015), thereby associated with mind wandering and internally directed self-related processing (Davey, Pujol, & Harrison, 2016). The DMN has yielded substantial evidence of functional markers of clinical disorders, among them schizophrenia, opioid addiction (Ma et al., 2015; Razi, Kahan, Keen, & Friston, 2015) and chronic pain (Becker, Vogt, & Ibinson, 2018).

This has been of great interest for the clinical neurosciences, as psychiatric and neurological conditions are reflected in aberrations in functional connectivity, which can be analyzed on a topological level in deflecting graph theoretical properties: to this day, graph theoretical rs-fcMRI has yielded substantial insights in neuronal network organization in psychiatric or neurologically affected individuals and has provided biomarkers for various clinical conditions (Alexander-Bloch, Bassett, & Ross, 2018; DelEtoile & Adeli, 2017; Fornito, Zalesky, & Breakspear, 2015; Makovac et al., 2018). Thereby, research on graph theoretical functional connectivity made apparent that this framework holds high potential in modeling brain network organization and quantifying pathological aberrations (Caeyenberghs et al., 2017).

Graph theoretical parameters can be divided into two categories: functional segregation and functional integration. Functional segregation describes the brain's ability to dynamically access functionally specialized clusters in the network (Rubinov & Sporns, 2010) and describes the brain's capability to dynamically process information by engaging functionally distinct brain loci (Lord, Stevner, Deco, & Kringelbach, 2017). Functional integration refers to the ability to dynamically and rapidly combine and integrate chunks of information from distributed regions of the brain. Measures of functional integration represent the facility of brain regions to share information by integrating neuronal clusters. Together, functional segregation and integration dynamically form interrelating modes involved in cognitive functioning pertaining to cognitive demands (Cohen & D'Esposito, 2016). For example, Cohen and D'Esposito (2016) were able to demonstrate that, during a working memory task, network integration increased.

Yet, previous literature has only scarcely drawn upon graph theoretical measures in the framework of functional segregation or integration, as well as their connection to behavior (Cohen & D'Esposito, 2016). Thus, especially with resting state being deprived of behavioral markers, it remains considerably difficult to draw specific conclusions concerning graph theoretical measures and their link to behavior.

Machine Learning of Graph Theoretical and Functional Connectivity Measures

With applications in various industrial and scientific fields (Durstewitz et al., 2019), ranging from object or pattern recognition to precision oncology (Ding, Chen, Cooper, Young, & Lu, 2018), Machine Learning (ML), up until today, has risen to form an indispensable part of our lives. ML models, including deep neural nets (DNN), have also grown increasingly popular in the neurosciences, partly due to their ability to perform well in high dimensional data (LeCun, Bengio, & Hinton, 2015). In retrospect, ML and classification techniques such as Support Vector Machine (SVM), Naïve Bayes (NB) or *k*-nearest neighbor (kNN) classification have a long tradition in the neurosciences (Durstewitz et al, 2019). Yet, DNN outperform these rather simple algorithms, partly due to their ability of operating in high dimensional space.

This growing interest in ML has contributed to a novel and broadened understanding of neuroimaging data (Pereira, Mitchell, & Botvinick, 2009) and, among others, since has been employed for the automated classification of clinical populations, or the prediction of the course of neurodegenerative diseases (Hojjati, Ebrahimzadeh, Khazaee, & Babajani-Feremi, 2017). Thus, DNN can ultimately be used for predictions on the single subject level (Vieira, Pinaya, & Mechelli, 2017, for review).

Tying to that, ML entails great potential for diagnosis and prognosis in the face of neurological and psychiatric diseases (Fornito & Zalesky, 2018; Janssen et al., 2018), contributing to the development of individualized, tailored therapeutic interventions for patients (Cocchi & Zalesky, 2018). Yet, the neurosciences' application of this method for translational purposes such as in precision psychiatry is still in its beginnings, and open questions concerning, for example, the diagnostic sensitivity or overfitting of models are still a matter of current investigation (Walter et al., 2018). Altogether, although ML in the neurosciences is still 'in its infancy', this approach holds great promises for the future (Walter et al., 2018).

Apart from functional imaging data, ML also has been combined with Graph Theory to characterize functional connectivity parameters and to classify neuropsychiatric patients (Sato et al., 2018; Sacchet, Prasad, Foland-Ross, Thompson, & Gotlib, 2015).

Generally, DNN are biologically inspired ML models which, among others, can be employed for classification tasks, coined under the term of supervised learning. In supervised learning, the task of a system is to classify input data. This, for example, can be achieved by a feedforward DNN consisting of input, middle, and output layers. Information enters the input layer and is directed to the hidden layers, where the signal is weighted and allocated to a generally nonlinear transformation function, usually the rectified linear unit (ReLU) (LeCun et al., 2015). Subsequently, the output layer processes the weighted sum of the signals of the former hidden layer, transformed by the activation function (Trenn, 2008). A Multi-Layer Perceptron (MLP), an instance of a DNN, is an example for a supervised feed-forward DNN, which we employ in the current investigation.

In general, DNN learning is applied to a training and, afterwards, a test data set: first, training data is extracted from the dataset, which is then allocated to the system for classification purposes. An objective function thereafter computes the emerging error between predicted and actual result, which results in an adjustment of modifiable parameters, called weights (LeCun et al., 2015). Subsequently, a gradient vector is used to infer to the proper modification of the weights, such that the error is minimized. A commonly used gradient vector is the stochastic gradient descent (SGD), which, for a fraction of training data points, computes the average gradient of these training data points and accordingly adjusts the weights. This procedure is repeated until the mean of the objective function stagnates (i.e., does not decrease anymore) (LeCun et al., 2015).

ML for rs-fMRI can be especially useful to obtain evidence pertaining to prediction accuracy, investigating the precision of group prediction in light of data, which allows to draw conclusions pertaining to the ease - or accuracy - of how an algorithm manages to represent data points (or, in other words, how well data points can be discriminated from each other according to their group label).

Naltrexone and its Modulating Effects on the Opioidergic System

Advanced insights into the neuronal and neurochemical underpinnings of brain regions and their functional interrelation have encouraged attempts to draw inferences on the neuronal mode of action of pharmaceutical agents in rs-fcMRI. This scientific approach, which was introduced as pharmacological fMRI (phfMRI) by Leslie and James (2000), mostly combines drug administration with a cognitive task, thereby manipulating the neurochemical system so as to derive information on cognitive or affective functioning (Leppä et al., 2006). Yet, despite task-based phfMRI has yielded considerable informational value, advances in research on the influences of neuropharmacological

agents on behavior of neuronal connectivity at rest can be seen as the foundation of understanding the most basic impact of a given thereapeutic compound at the neural level.

A pharmaceutical agent which frequently has been employed in the neurosciences, most prominently in phfMRI, is Naltrexone (NTX), a powerful, non-selective opioid receptor antagonist. NTX typically binds to μ, δ, and κ opioid receptors (Weerts et al., 2008), but is thought to most strongly favor μ-receptors (Ko et al., 1998). This compound displays a half-life of 4-9 hours, a peak plasma level of 1 hour (Verebey, Volavka, Mule, & Resnick, 1976), and blocks up to 80% of all μ-receptors, if a dose of 50 mg is administered (Lee et al., 1998). The opioid system plays a vital role in a variety of neuropsychological functions, and aberrations in it are thought to underly several psychiatric diseases, comprising major depression, substance-use disorders, or borderline-personality disorder (Polunina & Bryun, 2013; for a review on the role of the μ-receptor and the opioid system in emotions see Nummenmaa & Tuominen, 2018).

Underlining a probable role of NTX in affect regulation, in a PET-imaging study, Zubieta et al. (2003) demonstrated μ-receptor activation and deactivation to be strongly involved in the experience of positive and negative affect. These observations link to findings suggesting that NTX impact upon brain regions involved in integrative processing of, among others, reward, emotion, and cognition (Lukas et al., 2013). By means of demonstration, NTX tended to decrease the salience of rewarding cues (Lukas et al., 2013), possibly due to proliferated engagement of frontal regions over salience attribution, and weakened functional connectivity between precuneus and sensorimotor areas (Courtney, Ghahremani, & Ray, 2016). Moreover, NTX was shown to reduce a cue-related, reward-like neuronal response to drug or food (Langleben et al., 2011; Murray et al., 2014). On an inter-individual level, NTX has been found to largely modulate the reward value of social and non-social cues (Mallik, Chanda, & Levitin, 2017; Wardle, Bershad, & de Wit, 2016) and to decrease the feeling of social connectedness (Inagaki et al., 2016). Interestingly, NTX has also been shown to reverse or normalize opioid induced reduced empathy for another's pain (Rütgen et al., 2015).

Regions of Interest for Naltrexone-Induced Neuronal Modulation

Opioid receptors are distributed across the whole brain, but some areas display a higher opioid receptor density than others, including the cingulate cortex (CC), the insula (INS), the precuneus, and the frontoparietal operculum (Baumgärtner et al., 2006; Leppä et al., 2006). Apart from that, the medial prefrontal cortex (mPFC) is considered as a major opioid binding area (Jones et al., 1991). In subjects affected by substance-use disorder,

NTX has been found to modulate the mPFC, a region strongly involved in self-related processing such as inhibition and emotional inference to another person's state of mind (Wang et al., 2015), as well as in working memory of emotional content (Smith et al., 2018) and empathy for pain (Lamm, Decety, & Singer, 2011). Furthermore, research suggests that the mPFC plays a vital role in withdrawal of opioids, whereby a hypo-functionality of this area may link to reward deficiency and a diminished inhibition of striatal areas. An upregulation of the mPFC might reduce craving and negative affect (Wang et al., 2015).

The anterior CC (aCC) is engaged in social cognition (Apps, Rushworth, & Chang, 2016), self-awareness and inhibitory control (Lou, Changeux, & Rosenstand, 2017), and plays a major role in empathy for another's pain (Bernhardt & Singer, 2012; Lamm et al., 2011). The posterior cingulate cortex (pCC), being among the most prominent binding sites for opioids (Leppä et al., 2006), is a densely connected central hub of the DMN (Leech & Sharp, 2014) and is involved in arousal (Boly et al., 2008, for review), as well as the processing of pain, reward and emotional stimuli (Maddock, Garett & Buonocore, 2003). For example, Wang et al. (2015) found the pCC to be an active reward-related region in response to drug-cues, and, together with the mPFC, to hold predictive value of therapy adherence in opioid addiction.

The INS is a key region for empathy and pain processing, whereby the anterior INS (aINS) is thought to play a major role in the affective processing of pain and vicariously sharing emotions (Bernhardt & Singer, 2012; Rütgen et al., 2015), whereas the posterior part of the INS (pINS) is thought to be majorly involved in pain processing (Vogt et al., 2018) and engaged in the sensory-discriminative domain of pain (Bernhardt & Singer, 2012). For example, no other brain region receives as much spinothalamic input as the pINS (Dum, Levinthal, & Strick, 2009), corroborated by evidence from lesion studies (Birklein, Rolke, & Müller-Forell, 2005) and fMRI findings showing an aberrated and pain intensity dependent connectivity from the pINS to the pCC in acute pain (Vogt et al., 2016; 2018). Also, the pINS is majorly engaged in reward (Wittmann, Leland, & Paulus, 2007).

The precuneus is suggested to play a major role in representation of the self (Cavanna & Trimble, 2006, for review), and is highly involved in empathy judgements (Chakrabarti, Bullmore, & Baron-Cohen, 2006). Crucially, the mPFC, INS, and CC form part of the DMN. Especially the mPFC, the precuneus, and the pCC have emerged as core regions of this network, as corroborated by PET and fMRI studies (Fransson & Marrelec, 2008).

Thus, for our present investigation, from the Dosenbach atlas (Dosenbach et al., 2010), we selected the mPFC, the INS, and the CC as core Regions of Interest (ROI).

Crucially, all these ROI are known to be actively engaged in pain and empathy processing while concurrently displaying a high opioid receptor density. As extended ROI, we additionally included the precuneus and the inferior frontal gyrus (IFG). Besides its mentioned involvement in empathy judgements, the precuneus anatomically exhibits mutual projections to areas relevant for pain processing, including the aCC, pCC, frontal cortex, and the putamen (Cavanna & Trimble, 2006, for review). Activation of the IFG was demonstrated during the processing of visual stimuli depicting faces in pain (Benuzzi et al., 2018), as well as in individuals experiencing painful stimuli (Brooks, Nurmikko, Bimson, Singh, & Roberts 2002). Nonetheless, in light of the whole-brain mechanism of action of NTX, most strongly favoring μ-receptors, we consider it as essential to also include whole-brain results from our graph theoretical, univariate and network-based analyses.

Rationale and Hypotheses of the Present Study

Research involving NTX as an opioid antagonist has mostly been conducted with clinical subgroups, and, if any, rather small sample sizes of healthy controls. To the best of our knowledge, no study to date has investigated the effects of NTX on functional connectivity in exclusively healthy participants entailing a sample of comparable size as recruited for the present investigation. With the current study, we aim to bridge this gap by means of a neuropharmacological rs-fcMRI investigation including a non-clinical sample receiving NTX or a placebo compound in a double-blind and randomized within-subject design. We thereby intend to converge information gained through different methodological angles to elucidate how NTX modulates neuronal connectivity on the level of functional or effective connectivity, as well as graph theoretical topological organization.

By that, we hope to contribute to an amplified understanding of the neurophysiological basis of NTX-induced neuronal modulations not only in ROI known to be actively engaged in empathy, social processing (i.e., processing pertaining to the inference of an other's mental state) and pain perception, but also on a whole-brain level. We strongly believe that our investigation will deepen our insights into the neural substrate of modes of action of this therapeutic compound, and particularly expect that our novel, multi-level approach will be of considerable interest for researchers in the clinical, social, cognitive and affective neurosciences, as well as for clinical practitioners alike.

On the basis of the aforemetioned empirical findings of the mode of action of NTX, as well as the neuronal and functional implications of ROI commonly identified as sensitive to this compound, we expect to find the following observations as a result of our current exploratory investigation:

a. Firstly, we expect that NTX will induce modulations in the functional connectivity and topological (graph theoretical) organization in INS and CC, which will differ between NTX and control condition (CON).

b. Secondly, we predict that NTX will induce modulations in neuronal connectivity between striatal areas and the mPFC, which will differ between NTX and CON (Wang et al., 2015).

c. Thirdly, we hypothesize that NTX will induce heightened neuronal activity in frontal regions, which will differ between NTX and CON.

d. Finally, we expect that the group label (NTX or CON) can be predicted by means of graph and functional measures as well as timeseries.

METHODS

Participants. In total, 42 participants (male: *n*=25, female: *n*=17) participated in the present investigation. At average, participants were 24 years old (mean=24.1 ± 3.24 years; male: mean=24.12 ± 3.38 years; female: mean=24.07 ± 3.32 years). Overall, 10 participants had to be excluded from further data analysis due to erroneous data, excessive movement during scanning, technical problems during the scanning procedure, or since they did not meet inclusion criteria.

Inclusion criteria. Inclusion criteria consisted of right handedness, normal or corrected to normal vision, common MRI safety criteria, as well as the absence of neurological or psychiatric disorders, or any physical condition or known intolerance to NTX and opioids (please see Appendix for a full summary of inclusion and MRI safety criteria). All participants underwent a clinical assessment by a trained physician and a urine drug test to ensure all inclusion criteria were sufficiently met.

Recruitment. Participants were recruited via online advertisement and received 45 Euro per session (90 Euro in total) as a monetary compensation in exchange for their study participation.

Experimental procedure. The study protocol was reviewed and approved by the Ethics Committee of the Medical University of Vienna and carried out in conformity with the Declaration of Helsinki (1964). Recruited prospective participants were invited for a medical clinical screening conducted by a physician to ensure no exclusion criteria, such

as psychiatric or neurological diseases, were met. Participants were informed about the rationale of the experiment, however, were told a cover story to ensure double-blind administration of NTX (see below). All participants gave written informed consent prior to taking part in the experiment.

Following a counterbalanced within-subjects design for the two fMRI scanning sessions, subjects were randomly assigned to either a CON or NTX condition. With an interval of at least one day after clinical screening, subjects were picked up at the entry of the University Clinic of Dentistry, Medical University of Vienna, and guided to the scanning facility. Subjects were asked to remove all metallic objects from their body and to fill out an MRI safety questionnaire. Subsequently, all subjects underwent a urine drug screening test, with female participants additionally undergoing a urine pregnancy test. If all inclusion criteria were met, subjects proceeded to undergo preparations for the task-based part of the experiment.

Administration of 50 mg NTX or placebo was conceiled by the aid of a cover-story, whereby the respective compound was presented as an fMRI signal enhancer entailing, if anything, very few side effects. Oral ingestion took place under visual inspection by the investigators, and participants were instructed to swallow the pill together with a sip of water. After pharmacological administration of 50 mg of NTX, participants waited for 45 minutes to ensure complete NTX absorption.

Resting State fMRI Data Acquisition and Processing

Resting State fMRI Scanning Protocol. FMRI Images were acquired with a 3T Siemens Magnetom Skyra MRI System (TR = 704 ms, TE = 34 ms, flip angle 50°, FOV 210 mm, voxel size 2.2 x 2.2 x 3.5 mm) with a multiband accelerated echoplanar imaging (EPI) sequence with a 32-channel head coil. Structural MRI data were collected using a magnetization-prepared rapid gradient-echo sequence (TR = 2300.0 ms, TE = 2.29 ms, 176 sagittal slices, voxel size 0.9 x 0.9 x 0.9 mm, FOV = 240 mm). Subjects underwent approximately 50 minutes of scanning. Resting state scanning was preceded by an empathy for pain task as described in Rütgen et al. (2015) and a novel emotion identification task. After resting state fMRI, a T1 measurement was conducted.

Preprocessing. Preprocessing was conducted via SPM12 (Wellcome Trust Centre for Neuroimaging, www.fil.ion.ucl.ac.uk/spm) with standard algorithms and parameters unless explicitly specified otherwise. Functional images were realigned to the first image of the first session and normalized to MNI stereotactic standard space using Diffeomorphic Anatomical Registration Through Exponentiated Lie Algebra (DARTEL; Ashburner, 2007)

using spatial smoothing (6-mm Gaussian kernel). Nuisance regression included cerebrospinal fluid (CSF), white matter (WM) and head movement parameters (HMP). CSF and WM were regressed out (Fox et al., 2005) and HMP were modeled with the Friston-24 model, an autoregressive moving average model which considers two timepoints (Friston et al.,1996; Power et al., 2015). To account for excessive head movement, volume censoring with framewise displacement (FD) threshold of 0.5 mm (Power et al., 2014) was applied. Volumes exceeding the FD threshold were removed. Volume censoring reduces motion induced noise and has been demonstrated to perform well (Parkes et al., 2015; Satterthwaite, 2013). Data were temporally band-pass filtered (0.01–0.1Hz) to account for low frequency drift and high frequency physiological noise signal. Z-standardization at subject level was applied which showed to reduce motion artefacts and noise induced by scrubbing (Van Dijk, Sabuncu, & Buckner, 2009).

Exploratory Whole Brain fMRI Analysis. To also consider differences between conditions on the voxel level, we conducted a whole brain fMRI analysis as implemented in SPM12 on an exploratory basis. First level analysis entailed motion parameters of subjects. A paired *t*-test as implemented in SPM12 was conducted. Thereby, we contrasted NTX against CON (NTX>CON) with results corrected for FWE (p <.05). Subsequently, we created a brain mask with the SPM Anatomy Toolbox (version 2.2.c) (http://www.fzjuelich.de/inm/inm1/DE/Forschung/_docs/SPMAnatomyToolbox/SPMAnatomyToolbox_node.html) for improved display of results. Because of distortions in the DARTEL masks, possibly due to failed registration processes, five subjects had to be excluded (n=37 subjects were included in our analysis).

Network Construction

Atlas-Based ROI Definition*.* Functional connectivity network construction was executed by means of the functionally defined Dosenbach Atlas (Dosenbach et al., 2010), as functionally defined atlases have shown to yield greater test-retest reliability than anatomically defined ROI, as well as greater reliability of graph theoretical parameters (Cao et al., 2014). The Dosenbach Atlas comprises 160 distinct cortical, subcortical and cerebellar ROIs (radius of spheres=5mm) around the peak activation MNI coordinates engaged in multiple brain functions previously identified based on comprehensive meta-analyses (Dosenbach et al., 2006; 2010). These regions are associated to six networks, including the default-mode, sensorimotor, fronto-parietal, cingulo-opercular, occipital and cerebellar networks.

Adjacency Matrices. The construction of adjacency matrices followed standard procedures as previously described (Braun et al., 2012; Power et al., 2011; Rubinov & Sporns, 2010; Wang et al., 2011). Mean time-series of 160 whole brain nodes were extracted by obtaining mean time-series of all voxels inside the ROI sphere (Wang et al., 2011). Edge construction was conducted via ROI to ROI pearson correlation, yielding one adjacency matrix per subject and session. Adjacency matrices were normalized by applying Fisher's *r* to *z* transformation for improved scalability. For group statistics, adjacency matrices per group were averaged, yielding one adjacency matrix per group.

Node Based Statistics

Node based statistics of the unweighted and directed adjacency matrices were derived by deploying the Network Based Statistics (NBS) (Zalesky, Fornito, & Bullmore, 2010). NBS aims at identifying connectivity differences in neuroimaging data of functional or structural networks (Zalesky et al., 2010). Similar as in mass univariate testing in, for example, SPM, NBS uses thresholding of statistical parametric maps at cluster level (Zalesky et al., 2010). This increases power of detecting networks, as conservative bonferroni correction has proven to be too conservative. Briefly, all edges are thresholded to construct a suprathreshold set of links. Next, topological clusters among the suprathreshold set of links are identified by comparing sizes of components to an empirical null distribution of maximal component size acquired by a permutation of group affiliation (Parkes et al., 2018). Resulting components structures are, at the level of the null hypothesis, completely rejected, not at the level of single connections. Finally, family wise error (FWE)-corrected *p*-values are assigned to each component using permutation testing (Zalesky et al., 2010).

Graph Theory Analysis

The mean time series for each subject were extracted with 160x160 regions according to the functionally defined Dosenbach atlas (Dosenbach et al., 2010). Then, a whole brain ROI-to-ROI correlation matrix using Pearson's *r* correlation was constructed and subsequently transformed to Fisher's Z matrices for improved scalability. Graph theoretical measures were conducted with the Brain Connectivity Toolbox (BCT) (Rubinov & Sporns, 2010; www.brain-connectivity-toolbox.net), as well as the Graph Theoretical Network Analysis Toolbox (GRETNA; https://www.nitrc.org/projects/gretna/; Wang et al., 2015) via MATLAB v17b. Measures derived via BCT and GRETNA were further processed with custom-made scripts via MATLAB v17b. Graph theoretical measures of NTX and CON sessions were tested for significance with a paired *t*-test with FDR-correction to account

for false-positives. Graph theoretical parameters were scaled as area under the curve (AUC; Wang et al., 2009; Zhang et al., 2011), which is a measure independent from thresholds or imaging modality and provides sensitivity to topological differences in brain networks (Achard & Bullmore, 2007; Wang et al., 2009).

Mean and Concatenated Group Analysis

Mean group analysis. A threshold of 0.15 was selected. As there is no consensus about the appropriate cutoff density to be chosen for a graph, it is suggested to consider a tradeoff between density and yet fully connected graphs. Referring to Braun et al. (2012), who restricted analysis to densities ranging from 0.1 to 0.4 and taking into account the presumably rather small effects of NTX in healthy populations (Morris et al., 2018), a density of 0.15 was selected as a reasonable tradeoff between sparse and connected graphs. A graph theoretical analysis entailing the averaged adjacency matrix per group (binarized with a 15% threshold and averaged) was used for a paired *t*-test (FDR-corrected).

Concatenated group analysis. For concatenated graph measures, single nodes of the Dosenbach Atlas (Dosenbach et al., 2010) were integrated (summarized) per region (i.e., all nodes of the posterior cingulate). Nodes entailed mPFC, INS and CC. On a coarse level, this allows for better generalization (and visualization) of measures of functional integration and segregation on ROI.

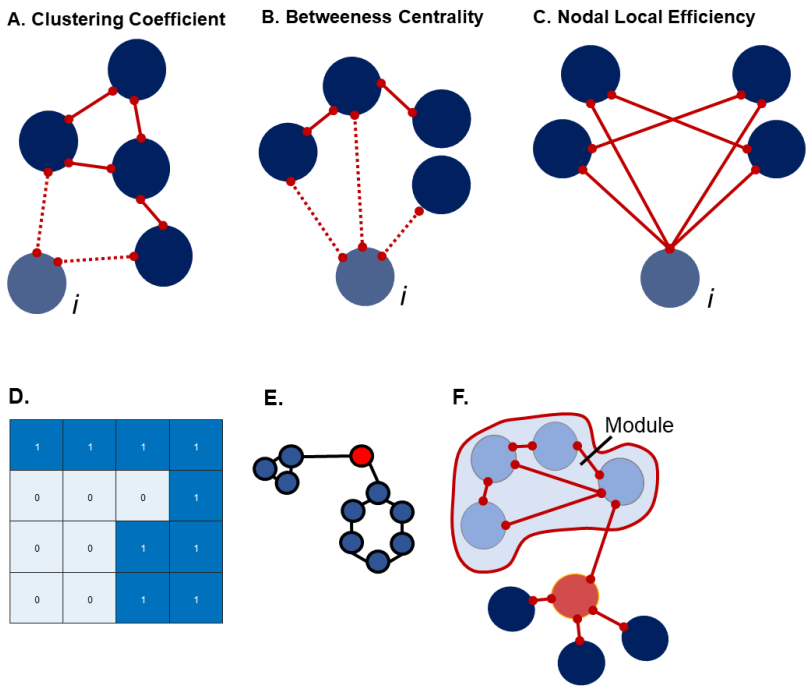

Figure 1. Display of three exemplary graph theoretical measures used in the present investigation. **A.** Display of the Clustering Coefficient measured as the ratio of number of connections between direct neighbors of node i and the maximum number of possible connections between the neighbors of *i*. **B.** Betweenness Centrality refers to the number of shortest paths of a network that cross through *i.* **C.** Nodal local efficiency is defined as the inverse of the harmonic mean of the minimum path length between a node *i* and all other nodes of the network. **D.** Depiction of the graph theoretical measure connected components. **E.** display of a graph with n=2 connected components. **F.** Display of the graph theoretical measure of modularity.

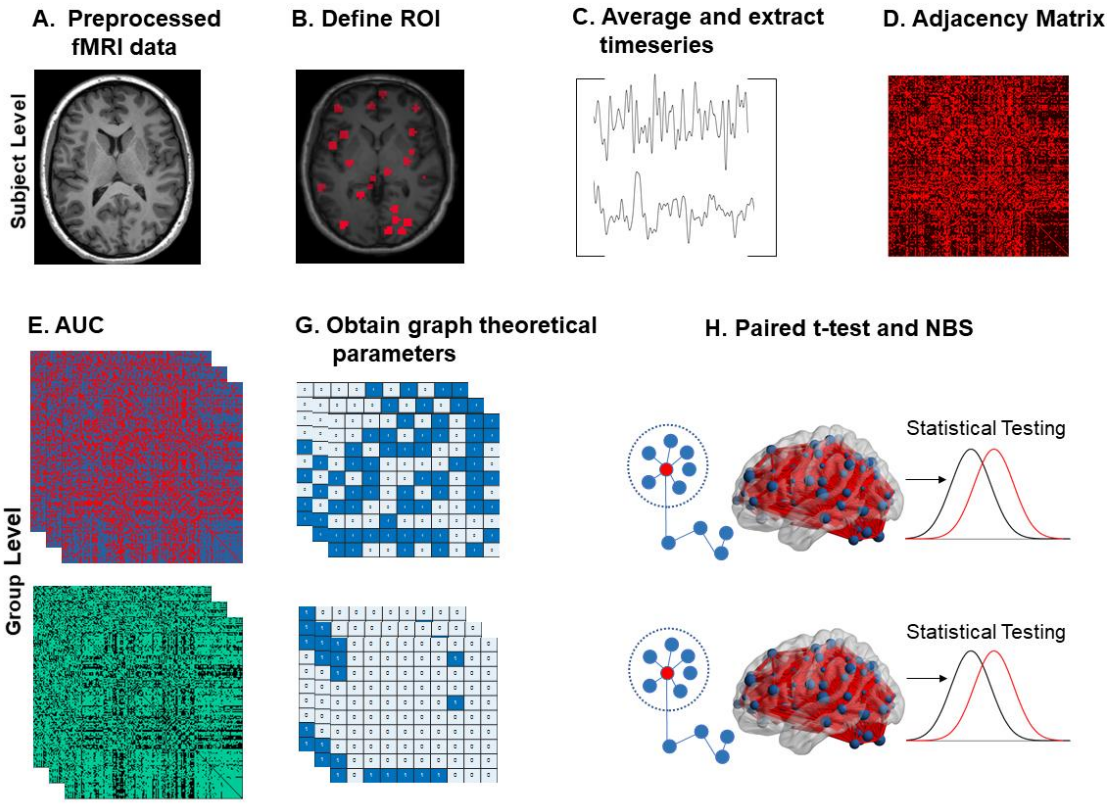

Figure 2. Display of the workflow of resting state functional connectivity and graph theoretical analysis. **A. – D.** MRI data is preprocessed, and regions of interest are defined. Subsequently, timeseries of the ROIs are extracted, followed by the construction of the adjacency matrices. **E.-G.** For Graph analysis, adjacency matrices are obtained as area under the curve. For Network Based Statistics, adjacency matrices are thresholded with a *t*-value. For graph theoretical parameter testing, values are tested with a paired t-test, FDR-corrected $p < .05$. For Network Based

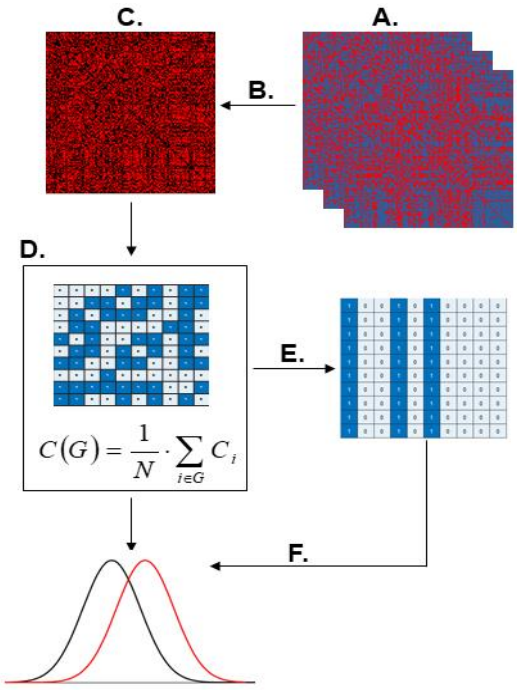

Figure 3. **A.** Subject-wise connectivity matrices are displayed. **B.** Connectivity matrices are averaged. **C.** This results in an average matrix per session (NTX/CON). **D.** Graph theoretical measures are drawn from the resulting averaged connectivity matrix. **E.** For probability density plots and graph theoretical node-wise analysis, subsets of nodes are combined to a region (e.g., all nodes of insula are combined to the node of anterior insula). **F.** These are subsequently tested with a paired t-test (FDR-corrected). *Note.* Displayed formula, clustering, is only depicted for means of demonstration.

Graph Theoretical Measures

Global Efficiency (AUC). Global efficiency is a measure of functional integration and measures the global efficiency of information flow within a network. Mathematically, global efficiency is the average inverse of the shortest path length, which infers to the minimum covered distance from one node to another (Bullmore & Sporns, 2010; Latori & Marchiori, 2001). Global efficiency is considered a very reliable measure of functional integration because it is not influenced by short paths (Archard & Bullmore, 2007).

Nodal Efficiency (AUC). Nodal efficiency is a measure of functional integration. It measures a nodes' capability of efficient information flow. Nodal efficiency is calculated as the average inverse of the shortest path length, whereby it captures the minimum covered distance from one node to another, as well as from all other nodes in the network (Bullmore & Sporns, 2010; Drakesmith et al., 2015; Latori & Marchiori, 2001).

Nodal Local Efficiency (AUC). Nodal Local Efficiency is a measure of functional segregation. It refers to the shortest path between a pair of nodes *i* and *j*, that only contains neighbors of node *i* (Rubinov and Sporns, 2010).

Nodal Cluster Coefficient (AUC). The nodal cluster coefficient is a measure of functional segregation. Brain regions with a high cluster coefficient are in an environment of other nodes that are highly connected to each other. The cluster coefficient of a node is the proportion of links between the node's neighbors and all possible links (Sporns, Chialvo, Kaiser, Hilgetag, 2004). In other words, the Cluster Coefficient describes the ratio of a node's neighbors that are themselves neighbors (Rubinov and Sporns, 2010), and thus describes the regional efficiency of information flow in the local neighborhood of a node (Watts & Strogatz, 1998).

Modularity*.* Modularity is a measure of functional segregation (Rubinov & Sporns, 2009) and reflects the community structure of a network. It refers to the degree to which a node forms a community with another node. A node with high modularity has dense connections to the node he resides in a community structure with, but more sparse connections with the other nodes (Newman, 2006).

Betweenness Centrality (AUC). Betweenness Centrality (BC) is a global measure of functional integration. Brain regions which serve as hubs, highly interconnected regions, facilitate functional network integration and resilience to attacks, and therefore display a high extent of centrality (Rubinov & Sporns, 2010). Brain nodes with BC participate in many short path links (Freeman, 1977; 1978). BC is formalized as the proportion of all shortest paths passing through a network node (Rubinov & Sporns, 2010).

Connected Components. Connected Components is a measure of clustering, which yields subnetworks of a node, in which all pairs of nodes are interconnected.

Spectral Dynamic Causal Modelling

Functional connectivity analysis entails inherent limitations, as correlations between regional time series of neurophysiologically remote regions do not allow for any kind of causal statement, thereby precluding inference on the directionality of neuronal activity. A recent development in the neurosciences to overcome the limitations of functional connectivity by allowing causal inference on neuronal connectivity is spectral Dynamic Causal Modelling (spDCM), which operates on the spectral density domain (Razi et al., 2015). Thereby, spDCM describes the causal influence one neural system exerts over the other, or, in other words, enables inference on the causality of functional connectivity. Briefly, spDCM allows for the investigation of effective connectivity between neural regions, including endogenous activity (Razi et al., 2015), rendering it especially useful for studying neuronal activity at rest. To complement the graph theoretical, node based and group-wise statistics used in the present investigation, a follow-up analysis employing a spDCM analysis of average effective connectivity measures was conducted (A-Matrix). ROI were selected in the light of graph theoretical and node-based measures, which is in line with the hypothesis-driven nature of DCM analyses (Stephan et al., 2010). Besides the core ROI, we included sensorimotor regions, as studies employing NTX often found induced modulations in sensorimotor regions, such as the inferior parietal lobule or the supplementary motor area (SMA) (Mann et al., 2014). This resulted in seven regions, which were subsequently allocated to the spDCM analysis. ROI were comprised of the medial PFC, right ACC, right pCC and bilateral INS, right precuneus and SMA.

Implementation. For spDCM analysis, the identical fMRI data was used that has been employed for graph theoretical and ML analyses (*n*=42 subjects).

Table 1 Regions of Interest for spectral DCM

ROI	Side	MNI		
		x	y	z
mPFC		0	51	32
aCC	R	9	39	20
pCC	R	1	-26	31
pINS	L	-30	-29	9
	R	42	-24	17
Precun	R	11	-68	42
SMA		0	-1	52

Note. Regions of Interest (Dosenbach, 2010) used for spDCM analysis (A-Matrix).

Machine Learning of Functional Connectivity and Graph Theoretical Parameters

Machine Learning of Connectivity Matrices and Timeseries.

We investigated the classification success of NTX vs CON session by employing a feedforward DNN with the functional connectivity matrices and timeseries.

Implementation of Deep Neural Network. DNN implementation was conducted with an Anaconda environment and Spyder 4 (Python 3.6). Further, the Python packages Scikit-learn (Pedregosa et al., 2011) and NumPy (Van der Walt, Colbert, & Varoqaux, 2011) were used for data preprocessing and analysis. Scikit-learn is a commonly used package in the neuroscientific machine learning field (Walter et al., 2018). In a first step, functional connectivity and timeseries were concatenated per group, resulting in 84x25600 (functional connectivity matrices) and 160x47866 (time series) matrices. Subsequently, data was randomly split into a training and a test set, which were used for training and testing of the DNN model, respectively. A Grid Search (optimizing free parameters) was conducted with GridSearchCV (as implemented in scikit learn). According to GridSearchCV output and inspection of the classification scores, hyperparameters were tuned, resulting in following specifications: size of hidden and output layers: 120,2; learning rate initiation: 0.0001; learning rate: constant; maximum iterations: 400; momentum: 0.3; solver: L-BFGS; tolerance: 0.000001; validation fraction: 0.1. Other parameters remained at standard specification as implemented in scikit-learn.

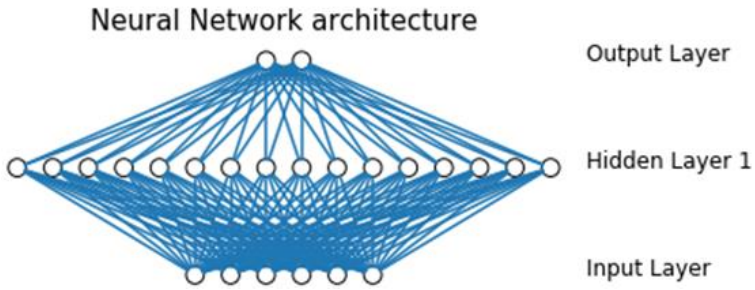

Figure 4. **A.** Simplified display of a neural network. Per layer, every node is interconnected to all other nodes. The input layers allocate the fed information to one or several hidden layers, where the information is weighted and subsequently fed to the output layers, where an activation function is applied.

Machine Learning Classification of Graph Theoretical Components.

To investigate the discriminative power of graph theoretical measures for group categorization, two ML classification algorithms were employed for classification of NTX or CON. The NB and *k*-nearest neighbor kNN algorithms have been employed regularly for classification tasks in the framework of rs-fMRI analysis (Khazaee et al., 2017). The NB classifier is a probabilistic approach to classification problems estimating conditional probabilities from features and labels (class allocation). This approach has been shown to perform very well in a variety of problems, including high dimensional space, which makes

it especially useful for analysis of rs-fMRI (Khazaee et al., 2017). The kNN algorithm classifies a test pattern according to majority class label of the *k*-nearest training patterns (Bishop, 2006). Generally, classifiers use a set of features to predict the associated class. Unsurprisingly, a function trained on a dataset which is identical with the test set would have a perfect accuracy score but, at the same time, fail to predict new data points. Therefore, the feature space is usually split into a training and a test set. Cross-validation is a ML technique used to evaluate model performance: A training data set is partitioned in *k* subsamples, which are subsequently used to predict the remaining data, therefore preventing overfitting. Subsequently, model performance can be measured by employing various model performance parameters. Misclassification rate is a commonly used measure of performance often employed in ML. The Misclassification rate refers to the classifier performance to predict new values in the test set: A Misclassification rate of 0 thus indicates an accuracy of 100%.

Implementation. NB and kNN classification were conducted with Anaconda environment, Spyder 4 (Python 3.6) and the Python packages Scikit-learn (Pedregosa et al., 2011) and NumPy (Van der Walt, Colbert, & Varoqaux, 2011). For classification, graph theoretical components were concatenated per group, resulting in 84x160 matrices per measure. After group label allocation, Naïve Bayes (with hyperparameter optimization) and *k*-nearest neighbor classification was implemented.

Follow-Up Correlational Analysis of Behavioral and Graph Theoretical Measures

To complement our previous analyses with behavioral markers, we conducted a correlation analysis (Pearson correlation) between graph theoretical measures which revealed significant alterations due to NTX administration and behavioral measures of experienced self-pain of a previous to the resting-state scanned empathy for pain task (described in detail in Rütgen et al., 2015). Briefly, this task consisted of either self- or other-directed pain stimulations, applied via an electrode on the right hand and rated on a Visual Analog Scale. Eighteen participants could not be included in our follow-up analysis, either because they failed to show up for the second session (n=4), interruption of the session (n=4), illogical pain ratings (for example, pain administration was rated as not painful), flawed fMRI data (n=2) or both (n=4). The final sample consisted of N=34 participants (female: n=19, age: *M*=23.5, S.E.M.=0.46).

RESULTS

Network Based Statistics

To identify regions at cluster level, a whole brain network based statistical analysis (NBS) paired *t*-test permutation test (contrast: NTX > CON, *n*=10000 rounds, threshold: *t*=3.5, *p*<.05 FWE corrected at cluster level) was conducted (please see Table 8 in the supplement for detailed information). NBS analysis yielded 4 networks. The first network (*p* <.01) entailed nodes such as the precuneus, pCC, medial insula (mINS), and ventromedial prefrontal cortex (vmPFC) projecting to thalamus, angular gyrus (AG) and pINS. Network 2 (*p*<.01) yielded nodes such as the dorsolateral prefrontal cortex (dlPFC), mPFC and extrastriate (occipital cortex) projecting to med cerebellum. In network 3 (*p*<.02) we found, among others, nodes of the superior frontal (sFC) and dorsolateral prefrontal cortex (dlPFC), projecting to medial frontal cortex (mFC). Network 4 (*p*<.003) yielded nodes such as the pCC, aINS, mINS, precuneus, projecting to mINS, pINS and temporal cortex.

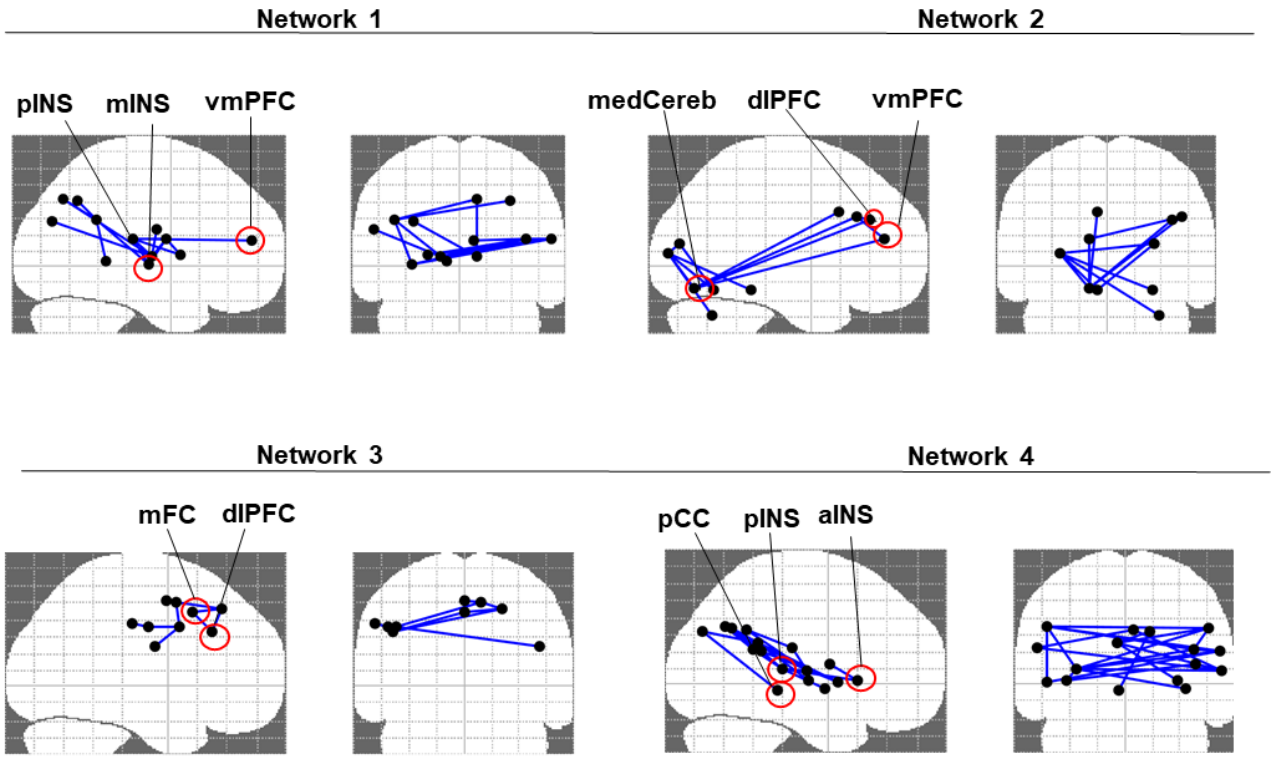

Figure 5. Display of the NBS analysis (*n*=10000 permutations, threshold *t*=3.5). NBS analysis yielded 4 subnetworks. *Note.* pINS= posterior insula; mINS=medial insula; aINS=anterior insula; vmPFC= ventromedial prefrontal cortex; medCereb=medial cerebellum; dlPFC= dorsalateral prefrontal cortex; pCC=posterior cingulate cortex.

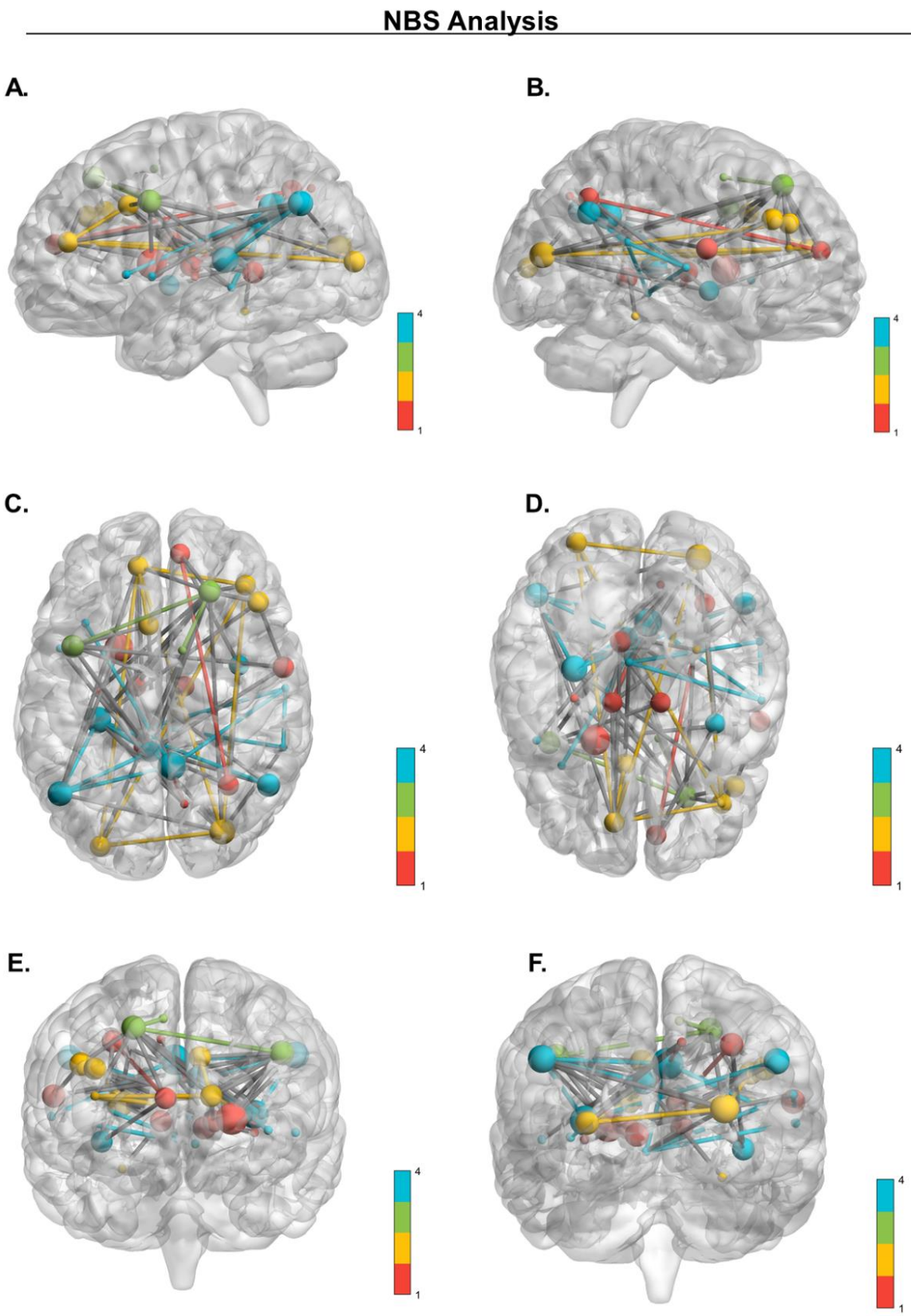

Figure 6. **A.** Display of NBS analysis (entailing 4 networks as displayed by the colorbars). Size of the nodes relate to *t*-values yielded by the NBS analysis. Display of **A.** left cerebral hemisphere; **B.** right cerebral hemisphere; **C.** top/dorsal view; **D.** bottom/ventral view; **E.** frontal/rostral view; **F.** back/caudal view. Visualized with BrainNetViewer (http://www.nitrc.org/projects/bnv/) (Xia, Wang & He, 2013).

Graph Theoretical Measures

Global Efficiency (AUC). Global Efficiency displayed no significant results (p>.95).

Nodal Efficiency (AUC). An FDR-corrected paired t-test revealed significant differences across sessions for a range of nodes. Besides sensory and motor areas, the mPFC (t= -3.39, p<.01) as well as the IFG (t= -5.34, p<.0001) significantly differed in nodal efficiency across condition (see Table 2). Further, INS (most prominently the left INS, t= 3.22, p<.001) and CC (left CC: t=-5.30, p<.0001) displayed significant aberrations between NTX and CON.

Nodal Local Efficiency (AUC). Nodal Local Efficiency was modulated between conditions in a variety of ROI, such as prefrontal, occipital, motor and sensory regions as well as the precuneus (t= -5.44, p<.001). Further, NTX showed a modulatory effect on the posterior insula (t= -3.04, p<.05) (see Table 2).

Nodal Cluster Coefficient (AUC). Of all calculated measures, the nodal cluster coefficient showed the widest range of significantly altered ROI entailing nodes in the frontal, temporal, parietal and occipital cortex. The frontal cortex contained significantly altered nodes comprising the mPFC (t=5.12, p<.0001), and, most prominently, the right IFG (t=8.39, p<.0001). Further, medial and posterior nodes of the INS revealed aberrations in nodal clustering across sessions, most prominently in the posterior right INS (t=-5.80, p<.0001). Nodes of the aCC and pCC also were significantly altered across sessions, most pronounced in the left pCC (t=5.76, p<.0001) (see Table 2).

Betweenness Centrality (AUC). Betweenness Centrality yielded no significant differences between sessions (p>.08).

Modularity. Modularity (weighted Adjacency Matrices) yielded no significant differences between sessions (p>.90).

Connected Components. Connected Components yielded no significant differences between sessions (p>.20).

Averaged Graph Theoretical Analysis. Group level graph measures were concatenated and fitted to a probability density function. Group parameter (AUC) of Nodal Cluster Coefficient revealed to be significantly different between two sessions (NAL: M= 0.24 ± 0.035 SD; CON: M=0.23 ± 0.03 SD, t=6.32, p<.0001, FDR-corrected). Nodal local efficiency (AUC) also showed significant modulations between sessions (NAL: M= 0.3 ± 0.02 SD; CON: M=0.33 ± 0.02 SD, t=6.32, p<.0001, FDR-corrected). Betweenness Centrality as well as Nodal Efficiency (AUC) displayed no significant alterations between conditions.

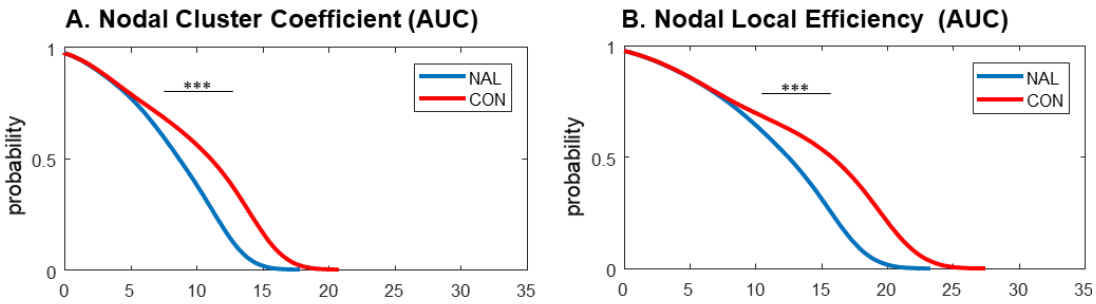

Figure 7. **A.** Display of the averaged group wise log-scaled probability density function (PDF) of the nodal cluster coefficient.

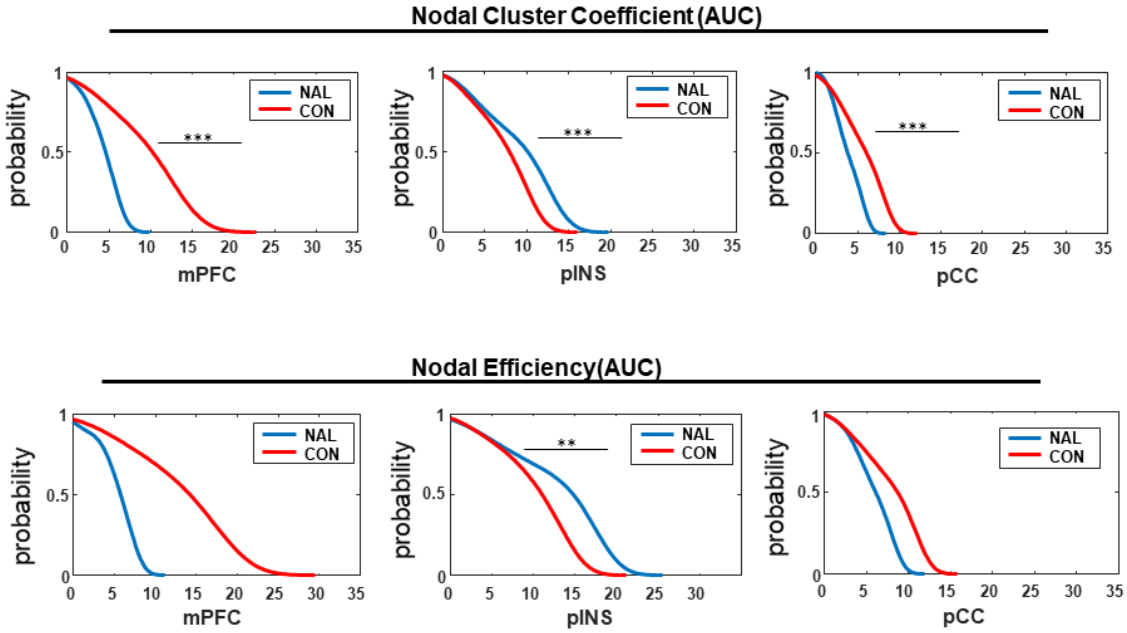

Figure 8. Display of the log-scaled probability density function (PDF) of the concatenated nodal cluster coefficient and nodal efficiency for posterior cingulate cortex (pCC) and posterior insula (pINS). *Note. See Supplement for statistical information.*

Table 2 Graph theoretical analysis

ROI	MNI			NAL		CON		t	p
	x	y	z	M	SD	M	SD		
Nodal Efficiency (AUC)									
mPFC	0	51	32	0.24	0.05	0.27	0.02	-3.39	<.01
vlPFC	46	39	-15	0.28	0.02	0.26	0.04	-5.34	<.0001
pINS	42	-24	17	0.27	0.01	0.26	0.03	3.07	<.05
mINS	-36	-12	15	0.26	0.03	0.22	0.06	3.68	<.01
pCC	-6	-56	29	0.25	0.02	0.27	0.02	-3.58	<.01
	5	-50	33	0.28	0.01	0.27	0.03	2.70	<.05
	-3	-38	45	0.27	0.02	0.26	0.03	3.65	<.01
	1	-26	31	0.24	0.04	0.27	0.02	-4.00	<.05
	10	-55	17	0.25	0.03	0.27	0.02	-4.13	<.01
	-11	-58	17	0.25	0.02	0.27	0.02	-5.30	<.0001
Precun	8	-40	50	0.26	0.02	0.25	0.03	2.86	<.05
Nodal Local Efficiency (AUC)									
vlPFC	46	39	-15	0.36	0.06	0.32	0.03	5.17	<.001
pINS	42	-24	17	0.33	0.02	0.35	0.03	-3.04	<.05
Precun	9	-43	25	0.30	0.02	0.31	0.03	-2.83	<.05
	11	-68	42	0.31	0.04	0.36	0.05	-5.44	<.001
Nodal Cluster Coefficient (AUC)									
mPFC	0	51	32	0.29	0.07	0.23	0.03	5.12	<.0001
vlPFC	46	39	-15	0.30	0.06	0.21	0.03	8.39	<.0001
mINS	37	-2	-3	0.23	0.04	0.27	0.07	-2.89	<.05
	-36	-12	15	0.27	0.04	0.34	0.09	-4.27	<.002
	32	-12	2	0.24	0.04	0.29	0.06	-4.82	<.001
pINS	42	-24	17	0.23	0.02	0.27	0.04	-5.80	<.0001
aCC	-1	28	40	0.25	0.03	0.28	0.06	-3.29	<.01
pCC	10	-55	17	0.28	0.07	0.24	0.03	3.90	<.01
	-11	-58	17	0.30	0.06	0.25	0.04	4.30	<.001
	-4	-31	-4	0.27	0.05	0.30	0.05	-3.46	<.01
	1	-26	31	0.28	0.06	0.25	0.04	3.75	<.01
	-5	-43	25	0.19	0.03	0.20	0.03	-3.01	<.05
Precun	8	-40	50	0.28	0.04	0.31	0.04	-4.30	<.001
	-6	-56	29	0.30	0.05	0.25	0.04	5.76	<.0001
	9	-43	25	0.18	0.02	0.20	0.03	-3.57	<.01
	11	-68	42	0.19	0.04	0.30	0.05	-8.28	<.0001

Table 2. Display of graph theoretical analysis. Statistical testing was conducted with a paired *t*-test (FDR-corrected). Note. Please see the supplement for the full list of significant ROI and abbreviations.

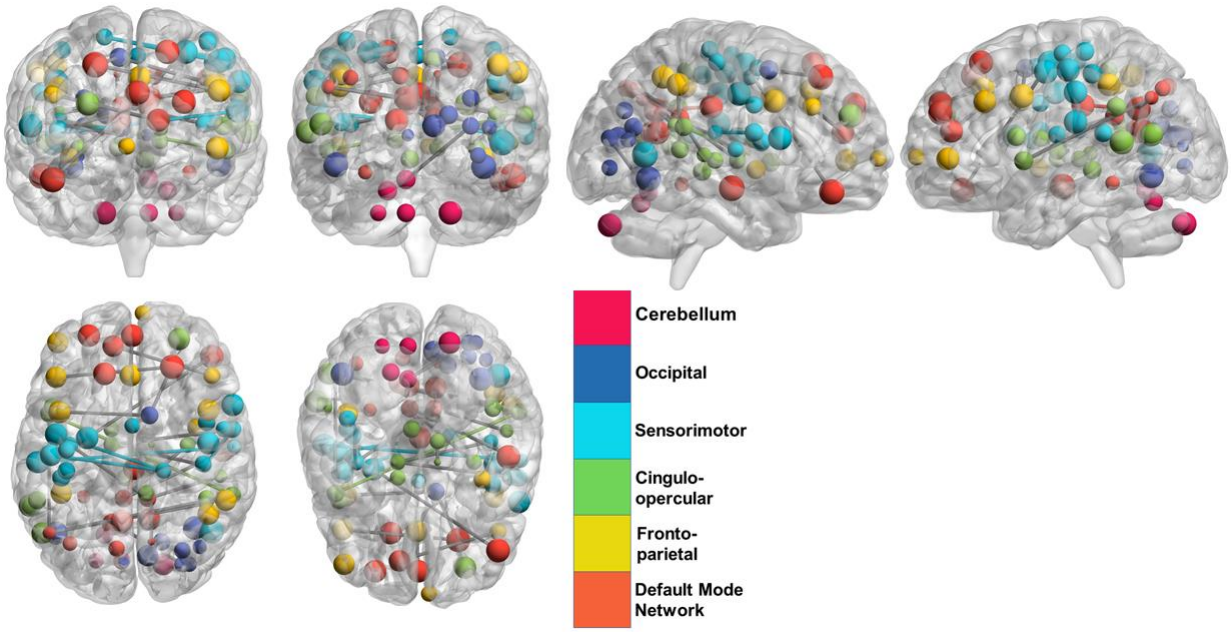

Figure 9. Display of the Nodal Cluster Coefficient (AUC). Node size indicate differences in nodal clustering *t*-values between conditions. Nodes represent significant modulations between condition in clustering with colour indicating the corresponding network. Edges between nodes relate to statistical differences in network-based statistics analysis (binarized). *Note.* Visualized with BrainNetViewer (http://www.nitrc.org/projects/bnv/) (Xia, et al., 2013).

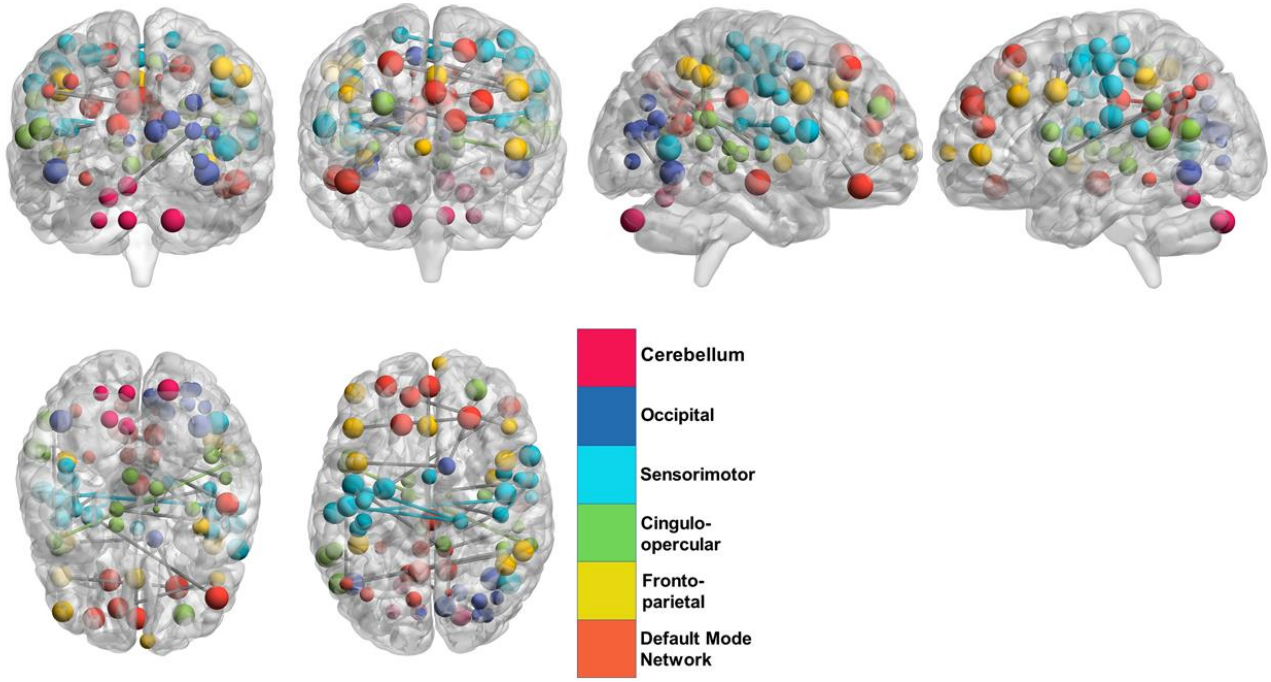

Figure 10. Display of the Nodal Efficiency (AUC). Display of the Nodal Efficiency (AUC). Node size indicate differences in nodal efficiency *t*-values between conditions. Nodes represent significant modulations between condition in clustering with colour indicating the corresponding network. Edges between nodes relate to statistical differences in network-based statistics analysis (binarized). *Note.* Visualized with BrainNetViewer (http://www.nitrc.org/projects/bnv/) (Xia, et al.,2013).

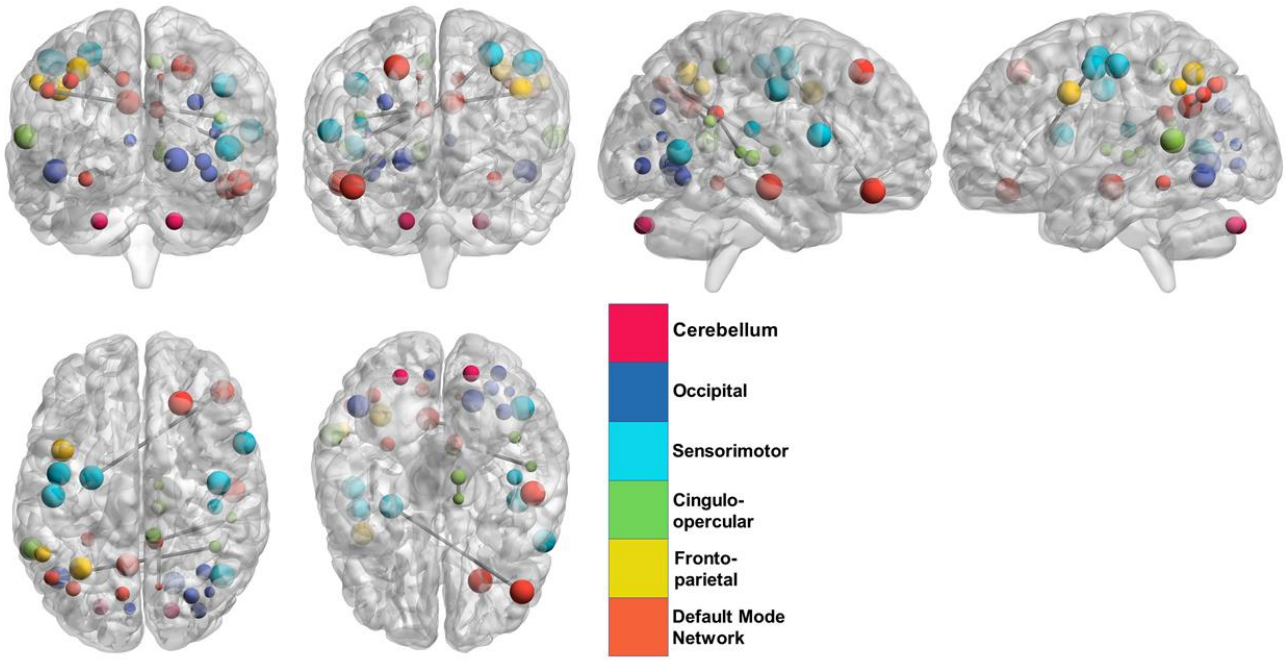

Figure 11. Display of the Nodal Local Efficiency (AUC). Node size indicate differences in nodal local efficiency *t*-values between conditions. Nodes represent significant modulations between condition in clustering with colour indicating the corresponding network. Edges between nodes relate to statistical differences in network-based statistics analysis (binarized). *Note.* Visualized with BrainNetViewer (http://www.nitrc.org/projects/bnv/) (Xia, et al., 2013).

Exploratory whole-brain fMRI analysis.

Univariate whole-brain fMRI analysis with contrast NTX>CON (FWE corrected, p <.05) revealed several activation clusters in frontal, parietal, occipital and cerebellar cortices (please see Table 9 in the supplement for detailed information). We found NTX induced upregulated functional connectivity in all core ROI. In general, especially the medial and dorsolateral PFC exhibited extended upregulation (mPFC, MNI: [-30,24,48]; dlPFC, MNI: [35,32,23]). Moreover, we found increased connectivity in temporal (planum temporale/auditory cortex, MNI: [48,-14,5]), subcortical (pINS, MNI: [-44,-14,51]; pCC, MNI: [12,14,21]; Thal, MNI: [-5,-8,17]), parietal (inferior parietal lobule (IPL), MNI: [-48,-30,35]; precuneus, (MNI: [-15,-41,44]) and cerebellar regions. In terms of peak activation, we observed the most pronounced effects in the periaqueductal grey (PAG) (MNI: [-6,-41,-15]).

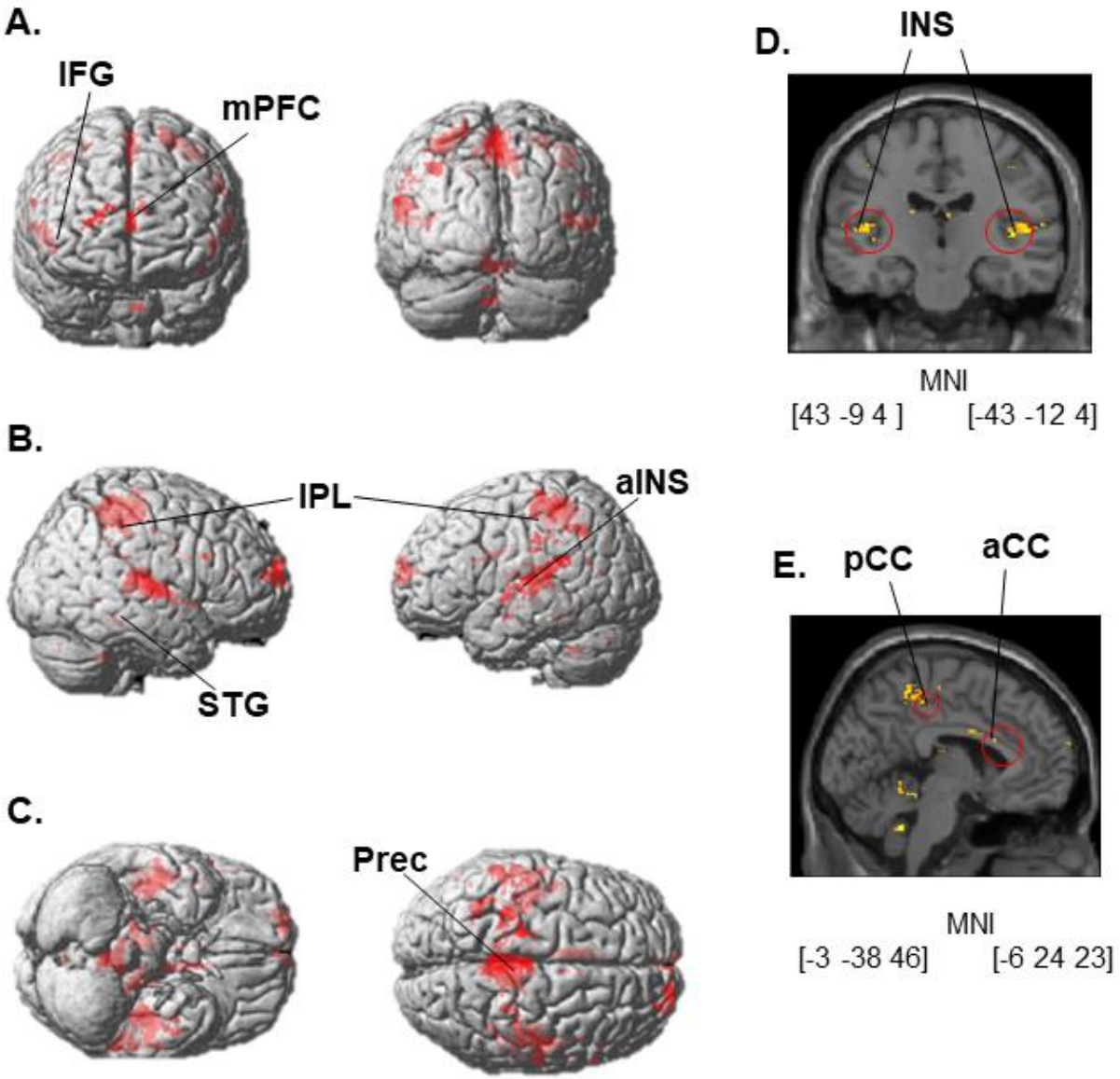

Figure 12. Display of whole-brain univariate fMRI group analysis NAL>CON (paired *t*-test, FWE-corrected p<.05) between conditions. Results were masked for ameliorated visualization with a mask created with the SPM anatomy toolbox. A. Rostral and caudal view displaying the IFG and mPFC. B. lateral view of the IPL, STG and aINS. C. Ventral and dorsal view displaying the Precuneus. D. transverse display of the aINS. E. Saggital view of the aCC and pCC. *Note*. Please see the supplement for detailed information.

Machine Learning of Functional Connectivity and Graph Theoretical Components

Machine Learning of functional connectivity. A DNN (MLP), an instance of a feedforward NN, was used for supervised classification of session (NTX or CON) for connectivity matrices and timeseries.

Connectivity Matrices and Timeseries. Connectivity matrices yielded a maximum accuracy score of 82.4%, however, accuracy scores displayed a high fluctuation and dependency from the random selection of training samples, thereby resulting in unsatisfactory reliability of prediction scores. DNN classification of neural timeseries resulted in a near to perfect accuracy score of 99.9%, remaining stable with the random selection of different training scores.

Machine Learning Classification of Graph Theoretical Components. Graph theoretical components revealed unsatisfactory classification performance of kNN and NB classification patterns (Accuracy scores for the nodal cluster coefficient: NB=0.15, kNN=0.46; Accuracy scores for Nodal Efficiency: NB=0.12, kNN=0.38; Accuracy scores for Nodal Local Efficiency: NB=0.11, kNN=0.54).

Spectral Dynamic Causal Modelling

Following graph theoretical analysis, a spDCM analysis was conducted. SpDCM analysis revealed average effective connectivity measures (A-Matrix) which displayed significant differences between sessions.

The connection of the left pINS to the right pCC as well as right pCC to mPFC revealed significant differences in effective connectivity between conditions (see Table 3 and Figure 13).

Table 3 spDCM analyses

***t*-Tests of Anatomical Effective Connectivity Matrices (A-Matrix)**										(df=41)
	MNI			MNI			M	SD	t	p
	x	y	z	X	y	y				
pINS > mPFC	42	-24	17	0	51	32				
NAL							0.0576	0.1456	2.33	<.05
CON							-0.027	0.21		
pINS > pCC	-30	-29	9	1	-26	31				
NAL							0.0119	0.0825	-2.813	<.01
CON							0.0671	0.107		

Table 3. Display of statistics of the effective connectivity values per condition. A paired *t*-test was conducted (p<.05, uncorrected).

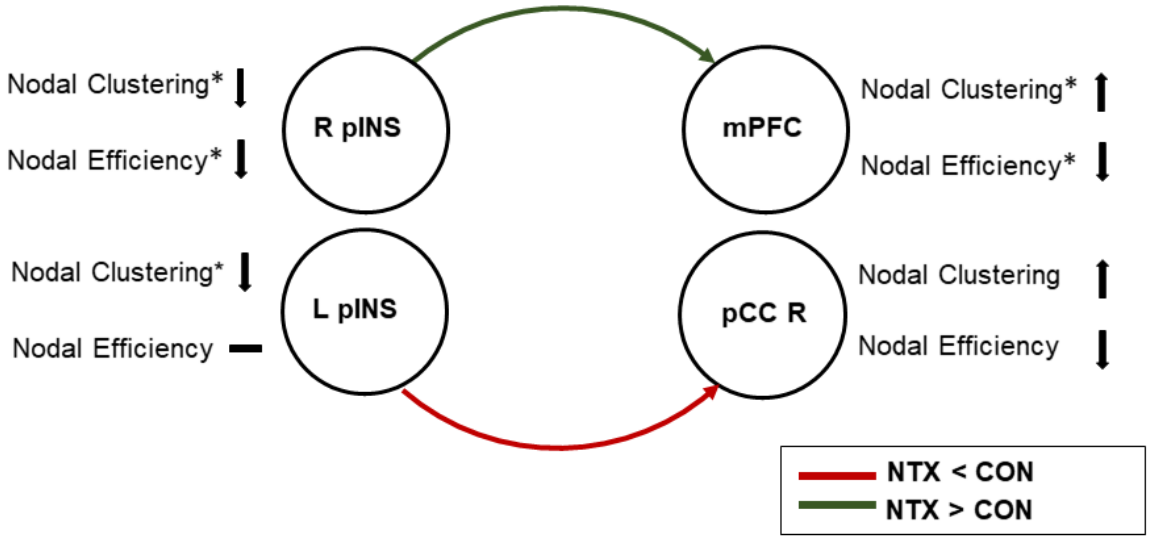

Figure 13. Display of A-Matrix effective connectivity connections between regions differing between conditions (*p* <.05) and graph measures. Graph measures marked with an asterisk differ significantly. Red lines indicate that the mean effective connectivity between sessions is lower in NTX as in CON. Asterisks indicate significant differences in Nodal Clustering or Efficiency between conditions. Nodal efficiency in the left pINS was equal between conditions.

Correlational Analysis of Behavioral and Graph Theoretical Measures

To investigate the relation between graph theoretical and behavioral markers, we performed Pearsons correlations between behavioral measures of experienced self-pain for NTX (please see the supplement for further information). A paired *t*-test revealed that self-pain significantly differed between NTX and CON (NTX: *M*=1.65, Std=1.41; CON: *M*= -2.89, Std=0.73, *t*=19.94, *p<.0001*). On a descriptive level, pain ratings were higher in CON than in NTX.

Table 4 Behavioral and graph theoretical correlation analysis

Nodal Cluster Coefficient (AUC)							
Region	**MNI**			**Mean**	**Std**	***R***	***p***
BG	-20	6	7	0.27	0.04	0.35	<.05
mINS	32	-12	2	0.19	0.02	0.33	<.05
PrecGyr	-54	-22	22	0.25	0.09	0.39	<.05
pINS	42	-24	17	0.23	0.10	0.42	<.01
Nodal Efficiency (AUC)							
BG	-20	6	7	0.35	0.035	0.50	<.001
PrecGyr	-54	-22	22	0.32	0.083	0.44	<.01
pINS	42	-24	17	0.29	0.11	0.43	<.01
postOccipital	-5	-80	9	0.31	0.029	0.32	<.05
Nodal Local Efficiency (AUC)							
vmPFC	-6	50	1	0.26	0.031	0.37	<.05
Occipital	-42	-76	26	0.26	0.027	0.46	<.01
BG	-20	6	7	0.26	0.021	0.38	<.01
vFC	-48	6	1	0.025	0.020	0.36	<.05
PrecGyr	-54	-22	22	0.024	0.057	0.51	<.001
pINS	42	-24	17	0.023	0.080	0.47	<.0.01
postOccipital	-5	-80	9	0.28	0.016	0.31	<.01

Table 4. Display of Pearsons correlation between graph theoretical measures and self pain for NTX. *Note. Please see the supplement for abbreviations and detailed information.*

DISCUSSION

Summary of Results

In this multi-methodological investigation, we conducted graph theoretical, functional and effective connectivity analyses conjoined with a ML approach to explore the neuronal effects of NTX. We found modulating effects of NTX in all analyses. On the most coarse (and least specific) level, we found that, on a global scale, NTX reduced functional integration as well as segregation. On the next, more specific level of concatenated ROI analysis, we discovered diverging effects of NTX, which reduced functional segregation (nodal clustering) and integration (nodal efficiency) in the mPFC, increased functional segregation and integration in the pINS, and reduced functional segregation in the pCC. Graph theoretically, we found extensive modulations in frontal, temporal, parietal, and to a lesser extent, occipital and cerebellar nodes besides our core ROI. These findings were solidified by our network-based analysis, which yielded increased functional connectivity in four distinct networks, entailing all core ROI and, additionally, the medial cerebellum, AG/IPL and extrastriate visual (occipital) cortex. Our univariate fMRI analysis corroborated these results by demonstrating increased functional connectivity entailing frontal cortex, INS, CC, precuneus. Furthermore, our findings demonstrated an increased functional connectivity in BG, Thal, transverse temporal gyrus, IPL and cerebellum.

Hypotheses. Hypothesis **a.** could be confirmed, whereby NTX, as compared to CON, induced modulations in graph theoretical, functional and effective connectivity measures in mPFC, IFG, INS, CC and precuneus. However, network-based analysis and univariate fMRI analysis indicated minor or insignificant NTX induced engagement of the IFG. Our results, however, were not in line with our Hypothesis **b.**, as we found no clear indications for modulations between striatal areas and mPFC. Nonetheless, our analyses showed increased functional connectivity in NTX in projections of basal ganglia/putamen to the right pINS. Confirming our expectations in Hypothesis **c.**, we found increased neuronal activity in frontal regions. Finally, our findings only partially supported Hypothesis **d.**, since functional connectivity and graph measures displayed unsatisfactory classification rates, whereas timeseries revealed a high classification rate according to a feedforward DNN approach.

Pertaining to concatenated and averaged group level, nodal local efficiency demonstrated few significant NTX induced alterations in regions on the concatenated level, but revealed several significant alterations on the averaged group level. This may be due to small effects, which indeed prevailed on a group level, but not at the level of

concatenated regions. However, on the level of single node graph theoretical analysis, nodal clustering and nodal efficiency showed the most extensive aberrations between conditions.

ML classification (by means of NB and kNN) of graph theoretical components yielded only unsatisfactory classification accuracies. This may be due to the subtle differences in graph theoretical measures between conditions. This argumentation is corroborated by visual inspection of data, revealing small differences between conditions. Both, NB and kNN, may thereby have met difficulty to discriminate between groups, as data points revealed to be rather narrow in size between conditions. Moreover, only specific nodes displayed significant differences between conditions. Employing all nodes of the Dosenbach Atlas (Dosenbach et al., 2010) for ML analyses may have introduced too much noise, resulting in an undermining effect on classification scores.

However, for timeseries classification, a feedforward DNN classification approach revealed an extremely high prediction accuracy of 99.9% classification performance, remaining stable with random selection of training data.This may be related to the ability of the DNN to represent data also in high dimensional space, thereby displaying boosted performance in representing even narrow differences between data points. Besides, the larger volume of training data may also have led to a higher classification accuracy, as subtle differences between conditions may be better represented by a higher volume of training data.

Relating to our network-based statistics analysis, we found four distinct subnetworks.The first network entailed several projections from the mINS, basal ganglia BG/Putamen and Thal to pINS. The second network displayed extensive projections from frontal and visual cortices to the medial cerebellum. The third network comprised several projections from the frontal cortex (superior frontal cortex (sFC) and dorsal frontal cortex (dFC)) to somatosensory network nodes, such as preSMA, SMA an Precentral Gyrus. Lastly, the fourth network consisted of multiple projections of the pCC, INS and AG/IPL. Among others, the pCC connected to AG/IPL and visual cortex, whereas the AG/IPL connected to pINS.

Concomittantly, univariate fMRI analysis largely confirmed findings of graph theoretical and network-based analysis. Our results revealed increased functional connectivity in frontal (mPFC, dlPFC), temporal (planum temporale/auditory cortex), parietal (IPL, precuneus), subcortical (pINS, pCC, Thal), and cerebellar regions. Especially the medial and dorsolateral PFC exhibited extended upregulation. Moreover, we observed significant neuronal upregulation in the left PAG.

With regard to our spDCM analysis, paired *t*-tests revealed aberrations in projections of the right pINS to mPFC and left pINS to right pCC. However, results did not achieve significance when FDR-corrected. This may be due to rather small modulations in effective connectivity between conditions, which indeed could be elicitied with functional and graph theoretical analyses, but did not prevail on the level of effective connectivity. For this reason, we presented uncorrected results in this part of our analysis, which, in an exploratory manner, remain only descriptive in nature. Follow-up investigations are warranted to validate and expand upon these findings. Yet, our uncorrected results are corroborated by graph theoretical, univariate and cluster based functional permutation testing (NBS). Thus, we argument that they allow, at least in an exploratory, descriptive manner and as combined with univariate, graph theoretical and network-based analysis, for a variety of interesting conclusions.

In addition to our previous task-free analyses, we also calculated Pearsons correlations between graph theoretical and behavioral measures of self-pain for NTX. For the nodal cluster coefficient (AUC), BG/Putamen, mINS and pINS were correlated with self-pain. For nodal efficiency (AUC), the same nodes as observed for nodal clustering, and additionally the visual cortex were associated with self-pain. For nodal local efficiency (AUC), we found small to medium Pearsons correlations entailing vFC, vmPFC, visual cortex, BG/Putamen and pINS.

General Discussion

Relating to previous research, our current findings are in line with previous findings pertaining to NTX inducing modulations in key regions eligible for reward, emotion processing and awareness (Lukas et al., 2013), linking to the multifaceted involvement of the opioidergic system in those areas. Although NTX is a non-selective opioid receptor (OR) antagonist, binding also to δ and κ receptors, it most prominently favors the μ-receptor (Wang et al., 2001). In general, the μ-receptor shows high densities in the Thal, prefrontal and CC, BG and midbrain structures, whereby the medial pain system displays higher μ-receptor densities than the lateral pain system (Sprenger, Berthele, Platzer, Boecker, & Tölle, 2005). Low μ-receptor densities are found in the occipital cortex and cerebellum (Frost et al., 1985). A study employing a μ-specific ligand by Leppä et al. (2006) found the strongest μ-binding capabilities in, among others, the aCC, pINS, mFG, IFG,precuneus, posterior parietal cortex (IPL), transverse temporal gyrus and Thal. Also, visual and auditory cortices display μ-OR capabilities (Quirion & Pipapil, 1991). For

example, Leppä et al. (2006) found that participants rated the scanner noise less irritating after remifentanil administration, pointing to μ-OR modulation in the auditory cortex.

Peak sites for δ-OR binding capabilities include the frontal cortex and putamen, whereas the Thal exhibited lower and the cerebellum absent δ-OR binding capabilities (Smith et al., 1999). The κ-OR exhibits the highest binding capabilities in the CC, striatum, frontal, temporal and parietal cortex, intermediate κ-OR binding capabilities in the Thal and medial temporal lobe and lowest binding capabilities in the brainstem and occipital cortex (Hiller & Fan, 1996).

Taking into account the pharmacological mode of action of NTX, we therefore had expected to find the most extensive neuronal modulation at μ-binding sites. Confirming the results of Leppä et al. (2006), who administrated a μ-specific opioid ligand, we found extensive NTX induced engagement of frontal (mPFC, dlPFC), temporal (transverse temporal cortex), parietal (precuneus, IPL), subcortical (INS, CC) and to a lower extent, occipital (visual cortex) and cerebellar nodes.

Pertaining to the OR specific peak sites, NTX induced engagement of the frontal cortical area related to μ, δ, and κ-OR. Further, the temporal and parietal cortex, specifically the transverse temporal gyrus/planum temporale and IPL, showed NTX induced upregulated neuronal activation. In line with Leppä et al. (2006), this points to mostly μ- and κ-OR bindings. NTX induced modulations in the occipital cortex, specifically in the visual cortex, relates to μ-specific binding, as δ and κ opioid OR show only insignificant binding in the occipital area. Concerning the cerebellum, we found few, but pronounced effects of NTX, which relate to mostly μ- and to a lower extent to κ-, but not to δ-opioid binding capabilities (Schadrack et al., 1999). Furthermore, we observed strong upregulated neuronal activity in the left PAG, which displays a high density of δ-OR (Ravert, Bencherif, Madar, & Frost, 2004).

Confirming our expectations, our analyses revealed NTX induced opioidergic modulations in regions engaged in the proprioceptive and affective coding of pain, self-other processing, empathy judgement and reward, wich differed between conditions. In our graph theoretical analyses, we found whole-brain NTX induced aberrations. Pertaining to our core ROI, our findings demonstrated graph theoretical modulations in the prefrontal cortex (PFC), anterior and posterior INS and CC as well as precuneus. In particular, we observed a pronounced alteration of the nodal cluster coefficient for between session effects of NTX.

These aberrations are corroborated by our univariate fMRI analysis (contrasting NTX>CON), revealing expected activation clusters in all core ROI. However, although the

IFG displayed upregulated neuronal activity induced by NTX, peak values indicated no strong NTX induced effects. Furthermore, we also found distinct areas of upregulated neuronal activity in temporal, parietal and occipital cortices. These entailed the AG/IPL, the auditory cortex/planum temporale, visual cortex and medial cerebellum.

These findings are further corroborated by our network-based analysis (NBS), which solidified previous analyses. Thereby, we found four distinct networks, which entailed our core ROI of medial frontal cortices (however, not the IFG), anterior and posterior nodes of the INS and CC as well as precuneus. Additionally, we found the Thal, transverse temporal gyrus/planum temporale, AG/IPL as well as the cerebellum in all our analyses to differ between conditions.

An observation of alterations in these additional nodes is plausible considering their functional specialization. For example, the right AG has been found to be engaged in the processing of rewarding cues (Guterstam et al., 2018), and the left AG as well as superior frontal cortices, such as the mFG/sFC, have been reportedly involved in pain related theory of mind (Jacoby, Bruneau, Koster-Hale, & Saxe, 2016). The IPL, being one of the least understood regions in the brain (Igelström & Graziano, 2017), is a major network hub of the DMN and engaged in higher-order cognitive capabilities as well as bottom-up perception and multimodal integration. Further, the IPL is involved in social cognition, self-awareness, introspection, and memory (Igelström & Graziano, 2017). For example, Decety and Lamm (2007) suggested that the IPL may contribute to social cognition by contributing to lower order processes pertaining to social cognition, such as attention and agency.

Moreover, the right Thal is part of the pain matrix (Jacobi et al., 2016), a major hub for afferent pain fibers (Wager et al., 2004), and counts among the peak regions of opioid induced neuronal activation (Nummenmaa et al., 2018). With regard to the temporal cortex, the transverse temporal gyrus/planum temporale exhibits strong opioidergic activation as found in PET investigation (Leppä et al., 2006). Apart from that, the right inferior temporal gyrus (IT) is a major opioid binding site (Leppä et al., 2006) and has also been reported to be altered in opioid addiction (Martin-Soelch et al., 2011). Together with motor and visual cortices, the IT is part of a set of regions apart from the mesolimbic pathway that mediates opioid activity (Martin-Soelch et al., 2001), forming an occipito-temporal visual attention network (Guterstam et al., 2018).

Pertaining to the cerebellum, the medial cerebellum displayed NTX induced aberrations in network-based analysis, graph theoretical and univariate fMRI analyses. This region has been found to be engaged in the processing of rewarding cues in

participants treated with NTX (Courtney et al., 2016), as well as in pain processing (Pomares, Faillenot, Barral, & Peyron, 2013).

In the first subnetwork (p<.01), the network-based analysis (NBS) revealed projections of the precuneus to right thalamus (Thal) and left AG/IPL as well as from BG/Putamen to pINS. Also, pCC and mINS projected to left AG (IPL). Graph theoretically, the left AG (IPL) displayed reduced functional segregation, but increased functional integration, and thereby exhibits increased connectedness to other nodes. This might indicate that this region may serve as a neuronal hub on a network level, also considering extensive projections of the left medial cerebellum and bilateral AG/IPL in several subnetworks. Moreover, the BG/Putamen to pINS projection functionally might represent a projection processing the affective coding of somatosensory integration, such as pain.

The second subnetwork (p<.01) most prominently revealed frontal (left mPFC, right dlPFC), extrastriate occipital and BG/Putamen projections to the left medial cerebellum. The third subnetwork (p<.02) yielded several projections between frontal nodes, such as the right mFG/sFC, and frontal nodes to supplementary motor area (SMA) and preSMA. In the fourth subnetwork (p<.003), we found projections of the pCC to the right AG (IPL), right mINS, extrastriate (occipital) and temporal cortices. Furthermore, the pINS displayed projections to temporal cortices. Again, left and right AG (IPL) displayed multiple projections to the left pINS and right superior temporal gyrus.

In our effective connectivity analysis, we observed an upregulated effective connectivity of the right pINS to mPFC and downregulated effective connectivity of left pINS to right pCC. Bilateral pINS displayed reduced functional segregation, whereas the mPFC displayed increased functional segregation. NTX induced upregulation of the right pINS to mPFC projection connection might link to the opioid antagonistic effects of NTX, leading to reduced reward (presumably resulting in reduced craving) and negative affect (Wang et al., 2015). Thereby, our analyses may suggest an opioidergic modulation of the pINS-pCC axis, which has been used to infer pain intensity and the existence of painful states (Becker, Vogt, & Ibinson, 2018). In line with this, it could be argued that an opioidergic downregulation of this pathway may result in a reduced integration of somatosensory pain signaling in self/other processing and awareness of not only one's own, but also another's pain.

With regard to the processing of one's own pain, we found small to medium Pearsons correlations between graph theoretical and behavioral measures of self pain. Thereby, nodal clustering (AUC) of mINS, pINS and BG/Putamen correlated with measures of self-pain. Our analysis of nodal efficiency (AUC) yielded the identical regions,

and additionally the visual cortex. Nodal local efficiency (AUC) revealed correlations between vFC, vmPFC, visual cortex, Putamen and pINS with measures of self-pain. In the context of experiencing (and anticipating) pain, it seems consistent that the neuronal engagement of pain (mINS, pINS) and emotion (BG/Putamen) processing areas leads to a shift in the allocation of neuronal resources to areas involved in anticipating and processing pain, leading to an ameliorated information processing capability of these areas. Graph theoretically, mINS and pINS displayed reduced clustering and nodal local efficiency (i.e, reduced informations segregation), but heightened nodal efficiency (i.e., increased information integration). This finding points to a heightened ability of information integration of the pain processing medial and posterior parts of the INS.

Presumably, lowered clustering (information segregation) but heightened efficiency (information integration) might be markers of the NTX induced hypoalgesia. In this perspective, a lowered capability of information segregation might lead to a lower likelihood of reciprocal projections and closed reciprocal loops, inducing enhanced distribution of information across networks (Morris et al., 2017; Sporns et al., 2004). Thereby, a heightened ability of information flow and dispersion might lead to a modulated processing of pain in the medial pain system, creating more neuronal flexibility. This could lead to a heightened influence of other networks (i.e., somatosensory network), inducing modulated -in our case, reduced- levels of pain.

This paradoxical effect of NTX on pain ratings in healthy individuals is a known characteristic (France et al., 2007). NTX displays high variability and low reliability in its OR-antagonistic effects. For example, NTX displays variable effects in studies employing pain ratings as a primary measurement; there may be no significant effect on pain ratings or, as in our study, paradoxically reduced pain ratings (for review see Werner, Pereira, Anderson & Dahl, 2015).

Within the scope of research on NTX, the visual system is thought to play a major role in reward mediation (Mann et al., 2014). Based on our findings, we can confirm NTX induced increased engagement of the extrastriate occipital cortex, which exhibited several projections to the medial cerebellum. Also, we found projections of the left pCC to the right extrastriate occipital cortex. In their study, Mann et al. (2014) investigated reward in a cued fMRI paradigm entailing detoxified participants affected by alcohol use disorder. Among others, they found a higher neuronal activation compared to controls in the temporal gyrus, AG/IPL, mFG, aCC, IT, INS and thalamus. Based on our analyses, NTX showed a modulation of neuronal activity in the abovementioned regions, engaged in rewarding cue reactivity. Contrary to previous research (Boettiger et al., 2009; Mann et al., 2014; Murray

et al., 2014), however, we found no strong evidence for the involvement of the orbitofrontal area. Although we found graph theoretical modulations in this area, NBS and fMRI analyses did not yield conclusive evidence for an NTX induced involvement of the orbitofrontal cortex. This may be due to the fact that most prior research on NTX involved clinical populations as participants. In these populations, NTX may have accentuated effects on some regions such as the orbitofrontal cortex.

Considering the effect of NTX on reward, it has been proposed that NTX may strengthen frontal regulation over salience attribution and the connectivity between precuneus and frontal regions, thereby affecting subjective craving (Courtney et al., 2016, for review). Indeed, our results indicate NTX induced connectivity modulations in the precuneus and frontal regions. However, network-based analysis yielded no evidence for a strengthened connectivity between precuneus and frontal regions, but to the right thalamus and left AG/IPL, and, with a more liberal *t*-threshold (*t*=3.0), increasingly to temporal regions. However, univariate fMRI yielded extensive NTX induced upregulated neuronal connectivity in the frontal cortex (mPFC, dlPFC), which might point to NTX induced increased frontal regulation.

Courtney et al. (2016) further proposed that NTX may reduce the salience of rewarding cues by decreasing the engagement of sensorimotor regions. Graph theoretical and network-based analysis (NBS) yielded no evidence to support this notion. Concerning sensorimotor engagement, we found increased connectivity of the SMA and the preSMA, receiving input from frontal regions.

Relating to Lukas et al. (2013), our findings confirm that NTX modulates areas key in reward, self-other processing, awareness and somatosensory proprioceptive integration. Besides our core ROI (mPFC, precuneus, CC, INS), the transverse temporal gyrus/planum temporale, bilateral AG/IPL, thalamus, putamen, PAG and medial cerebellum displayed significant NTX induced modulations. Thereby, we can confirm that NTX affects not only core regions of the pain matrix, such as the pCC, pINS and thalamus, but also distinct regions in parietal, temporal and occipital cortex (AG/IPL, transverse temporal gyrus/planum temporale, and extrastriate (occipital) regions) which can be allocated to the DMN. These findings point out that NTX seems to exert significant influence on DMN areas. Besides core regions of the pain matrix, which we reported to be engaged in NTX in line with our expectations, we found extensive activation of the occipito-temporal visual attention network (Guterstam et al., 2018), entailing temporal (IT, transverse temporal gyrus), extrastriate (occipital) and parietal (AG/IPL) regions.

In line with Rütgen et al. (2015 & 2018), who found NTX to reverse opioid induced reduced empathy for pain, NTX might annulate an opioid induced hampered awareness of experiencing pain by downregulation of, for example, the pINS-pCC pathway. Moreover, connections between the IPL and pINS might point to modulations between areas eligible for somatosensory integration, reward and empathy judgement.

Limitations. Despite our novel and integrative methodical approach, our study is not free of limitations, which we want to briefly mention in the following section. Firstly, because the resting state scan was part of a task-based fMRI study on empathy for pain, the scan was conducted approximately 2.5 hours after NTX administration. Considering the half-life of NTX of 4-9 hours and the peak plasma level of NTX at 1 hour (Verebey et al., 1976), stronger neuronal effects may have been observed, if the resting state scan would have taken place at the plasma peak of NTX (1-2 hours after administration).

Another implication of our study concerns the possible confounding influence of the task-based fMRI part of each scanning session, which were implemented prior to the resting-state. The previous scanned empathy for pain task, including the administration of pain stimuli, might have exerted longer lasting effects on neuronal activity. Thereby, a prior sensitizing of the pain matrix might have led to confounding neuronal activity in regions eligible for the processing of pain, but also empathy for pain. Pertaining to that, our novel emotion identification task, scanned prior to the resting-state, might similiarly have led to confounding neuronal activity in emotion processing areas.

In view of the pharmacological mode of action of NTX, effects are presumably not as pronounced in healthy subjects as in clinical populations, as evidenced by Morris et al. (2018). These authors found the most distinct effects in subjects affected by alcoholism relative to healthy individuals. Also, considering the bioavailability of NTX in oral administration of about 5-60% (Gonzalez & Brogden, 1988) very probably contributes to the ambiguous and unreliable effects of NTX on pain measures (Werner et al., 2015).

Another important factor concerns rs-fcMRI data sampling itself, as past research has found that the reliability of data significantly improves with scanning durations exceeding 10 minutes (Anderson, Ferguson, Lopez-Larson & Yurgelun-Todd, 2011). Moreover, even more scanning time may be necessary if one targets to discern an individual from the group, ranging from 25 minutes to 4 hours (Hacker et al., 2013).

Finally, it has to be accounted for the fact that our study, due to the limited prior knowledge base as to the effects of NTX in healthy individuals, was exploratory in nature and interpretations therefore need to be considered with caution. Yet, the present

investigation can be seen as a comprehensive foundation for future hypothesis-driven analyses, building up on the presented evidence gained through our seminal approach.

Future research. Taken together, our study revealed extensive findings allowing for multi-level insights into the effects of NTX on the whole brain. Based on our results, future research should consider larger sample sizes of healthy individuals, allowing for ameliorated reliability, which may be especially useful to account for baseline variability of metabolism and mode of action in pharmacological manipulations in experimental fMRI studies. Additionally, future research may consider the precise estimation of pharmacological modes of action, such as half-time or plasma peaks. Assing to that, research combining task-based with task-free paradigms was shown to considerably improve reliability and mapping of individual cognitive and behavioral markers (Elliott et al., 2019). Finally, the use of ML could deepen both reliability and validity of findings.

Taken together, the combination of topological with functional connectivity markers, as well as a biologically informed effective connectivity analysis entails great potential for an ameliorated understanding of neuronal connectivity. In this perspective, future research may further investigate the causal relationship between core areas of the pain matrix and extrastriate cortex, AG/IPL and medial cerebellum, which we found to be subject of significant NTX induced modulations.

Conclusion. Our presented investigation employed a powerful multimethodological framework, allowing for a multi-facetted perspective on the effects of NTX on neuronal connectivity of a sample of healthy individuals at rest, enabling a comprehensive description of both functional and topological levels of observation. We found aberrations in functional, effective and graph theoretical analyses in key regions eligible for somatosensory integration, reward, affective coding, pain and empathy for pain processing. Moreover, we showed that these regions can be allocated depending to their specific OR binding profile. Moreover, we observed that changes in the topological organization of brain areas, such as the striatum, medial and posterior INS, are linked to measures of experienced pain. By means of employing a ML approach, we demonstrated that graph theoretical parameters were insufficient when used for the classification of condition. In contrast to that, by means of a feedforward DNN approach, timeseries yielded very high accuracy when used for classification of condition. Taken together, our multimethodological framework provides important findings and explanatory power concerning the complex effects of NTX on neuronal activity of healthy participants at rest.

In that, we are confident that evidence gained by our seminal approach will immensely contribute to future research involving NTX.

REFERENCES

Achard, S., & Bullmore, E. (2007). Efficiency and cost of economical brain functional networks. *PLoS computational biology*, *3*(2), e17.

Alexander-Bloch, A. F., Bassett, D. S., & Ross, D. A. (2018). Missed Connections: A Network Approach to Understanding Psychiatric Illness. *Biological Psychiatry*, *84*(2), e9-e11.

Anderson, J. S., Ferguson, M. A., Lopez-Larson, M., & Yurgelun-Todd, D. (2011). Reproducibility of single-subject functional connectivity measurements. *American journal of neuroradiology*, *32*(3), 548-555.

Apps, M. A., Rushworth, M. F., & Chang, S. W. (2016). The anterior cingulate gyrus and social cognition: Tracking the motivation of others. *Neuron*, *90*(4), 692-707.

Azevedo, F. A., Carvalho, L. R., Grinberg, L. T., Farfel, J. M., Ferretti, R. E., Leite, R. E., ... & Herculano-Houzel, S. (2009). Equal numbers of neuronal and nonneuronal cells make the human brain an isometrically scaled-up primate brain. *Journal of Comparative Neurology*, *513*(5), 532-541.

Braun, U., Plichta, M. M., Esslinger, C., Sauer, C., Haddad, L., Grimm, O., ... & Walter, H. (2012). Test–retest reliability of resting-state connectivity network characteristics using fMRI and graph theoretical measures. *Neuroimage*, *59*(2), 1404-1412.

Braun, U., Schaefer, A., Betzel, R. F., Tost, H., Meyer-Lindenberg, A., & Bassett, D. S. (2018). From maps to multi-dimensional network mechanisms of mental disorders. *Neuron*, *97*(1), 14-31.

Becker, C. J., Vogt, K. M., & Ibinson, J. W. (2018). Human posterior insula to posterior cingulate functional connectivity is related to the subjective intensity of acute pain. *bioRxiv*, 246959.

Baumgärtner, U., Buchholz, H. G., Bellosevich, A., Magerl, W., Siessmeier, T., Rolke, R., ... & Henriksen, G. (2006). High opiate receptor binding potential in the human lateral pain system. *Neuroimage*, *30*(3), 692-699.

Benuzzi, F., Lui, F., Ardizzi, M., Ambrosecchia, M., Ballotta, D., Righi, S., ... & Porro, C. A. (2018). Pain mirrors: neural correlates of observing self or others' facial expressions of pain. *Frontiers in psychology*, *9*.

Bernhardt, B. C., & Singer, T. (2012). The neural basis of empathy. *Annual review of neuroscience*, *35*, 1-23.

Birklein, F., Rolke, R., & Müller-Forell, W. (2005). Isolated insular infarction eliminates contralateral cold, cold pain, and pinprick perception. *Neurology*, *65*(9), 1381-1381.

Bishop, C. M. (2006). Machine learning and pattern recognition. *Information Science and Statistics. Springer, Heidelberg*.

Boettiger, C. A., Kelley, E. A., Mitchell, J. M., D'esposito, M., & Fields, H. L. (2009). Now or Later? An fMRI study of the effects of endogenous opioid blockade on a decision-making network. *Pharmacology Biochemistry and Behavior*, *93*(3), 291-299.

Boly, M., Phillips, C., Tshibanda, L., Vanhaudenhuyse, A., Schabus, M., Dang-Vu, T. T., ... & Laureys, S. (2008). Intrinsic brain activity in altered states of consciousness: how conscious is the default mode of brain function?. *Annals of the New York Academy of Sciences*, *1129*(1), 119-129.

Brooks, J. C., Nurmikko, T. J., Bimson, W. E., Singh, K. D., & Roberts, N. (2002). fMRI of thermal pain: effects of stimulus laterality and attention. *Neuroimage*, *15*(2), 293-301.

Bullmore, E., & Sporns, O. (2009). Complex brain networks: Graph theoretical analysis of structural and functional systems. *Nature Reviews Neuroscience*, *10*(3), 186.

Bullmore, E., & Sporns, O. (2012). The economy of brain network organization. *Nature Reviews Neuroscience*, *13*(5), 336.

Cavanna, A. E., & Trimble, M. R. (2006). The precuneus: A review of its functional anatomy and behavioural correlates. *Brain*, *129*(3), 564-583.

Cao, H., Plichta, M. M., Schäfer, A., Haddad, L., Grimm, O., Schneider, M., ... & Tost, H. (2014). Test–retest reliability of fMRI-based graph theoretical properties during working memory, emotion processing, and resting state. *Neuroimage*, *84*, 888-900.

Chakrabarti, B., Bullmore, E., & Baron-Cohen, S. (2006). Empathizing with basic emotions: common and discrete neural substrates. *Social neuroscience*, *1*(3-4), 364-384.

Caeyenberghs, K., Verhelst, H., Clemente, A., & Wilson, P. H. (2017). Mapping the functional connectome in traumatic brain injury: What can graph metrics tell us?. *Neuroimage*, *160*, 113-123.

Cocchi, L., & Zalesky, A. (2018). Personalized transcranial magnetic stimulation in psychiatry. *Biological Psychiatry: Cognitive Neuroscience and Neuroimaging*, *3*(9), 731-741.

Cohen, J. R., & D'Esposito, M. (2016). The segregation and integration of distinct brain networks and their relationship to cognition. *Journal of Neuroscience*, *36*(48), 12083-12094.

Courtney, K. E., Ghahremani, D. G., & Ray, L. A. (2016). The effects of pharmacological opioid blockade on neural measures of drug cue-reactivity in humans. *Neuropsychopharmacology*, *41*(12), 2872.

Ding, M. Q., Chen, L., Cooper, G. F., Young, J. D., & Lu, X. (2018). Precision oncology beyond targeted therapy: Combining omics data with machine learning matches the majority of cancer cells to effective therapeutics. *Molecular Cancer Research*, *16*(2), 269-278.

Davey, C. G., Pujol, J., & Harrison, B. J. (2016). Mapping the self in the brain's default mode network. *NeuroImage*, *132*, 390-397.

DelEtoile, J., & Adeli, H. (2017). Graph theory and brain connectivity in Alzheimer's disease. *The Neuroscientist*, *23*(6), 616-626.

Dosenbach, N. U., Visscher, K. M., Palmer, E. D., Miezin, F. M., Wenger, K. K., Kang, H. C., ... & Petersen, S. E. (2006). A core system for the implementation of task sets. Neuron, 50(5), 799-812.

Dosenbach, N. U., Nardos, B., Cohen, A. L., Fair, D. A., Power, J. D., Church, J. A., ... & Barnes, K. A. (2010). Prediction of individual brain maturity using fMRI. *Science*, *329*(5997), 1358-1361.

Drakesmith, M., Caeyenberghs, K., Dutt, A., Lewis, G., David, A. S., & Jones, D. K. (2015). Overcoming the effects of false positives and threshold bias in graph theoretical analyses of neuroimaging data. *Neuroimage*, *118*, 313-333.

Dum, R. P., Levinthal, D. J., & Strick, P. L. (2009). The spinothalamic system targets motor and sensory areas in the cerebral cortex of monkeys. *Journal of Neuroscience*, *29*(45), 14223-14235.

Durstewitz, D., Koppe, G., & Meyer-Lindenberg, A. (2019). Deep neural networks in psychiatry. *Molecular psychiatry*, 1.

Elliott, M. L., Knodt, A. R., Cooke, M., Kim, M. J., Melzer, T. R., Keenan, R., ... & Moffitt, T. E. (2019). General Functional Connectivity: shared features of resting-state and task fMRI drive reliable and heritable individual differences in functional brain networks. *NeuroImage*, *189*, 516-532.

France, C. R., al'Absi, M., Ring, C., France, J. L., Harju, A., & Wittmers, L. E. (2007). Nociceptive flexion reflex and pain rating responses during endogenous opiate blockade with naltrexone in healthy young adults. Biological psychology, 75(1), 95-100.

Fransson, P., & Marrelec, G. (2008). The precuneus/posterior cingulate cortex plays a pivotal role in the default mode network: evidence from a partial correlation network analysis. *Neuroimage*, *42*(3), 1178-1184.

Freeman, L. C. (1977). A set of measures of centrality based on betweenness. *Sociometry*, 35-41.

Freeman, L. C. (1978). Centrality in social networks conceptual clarification. *Social networks*, *1*(3), 215-239.

Frost, J. J., Wagner, J. H., Dannals, R. F., Ravert, H. T., Links, J. M., Wilson, A. A., ... & Rosenbaum, A. E. (1985). Imaging opiate receptors in the human brain by positron tomography. *Journal of computer assisted tomography*, *9*(2), 231-236.

Fornito, A., Zalesky, A., & Breakspear, M. (2015). The connectomics of brain disorders. *Nature Reviews Neuroscience*, *16*(3), 159.

Fox, M. D., Snyder, A. Z., Vincent, J. L., Corbetta, M., Van Essen, D. C., & Raichle, M. E. (2005). The human brain is intrinsically organized into dynamic, anticorrelated functional networks. *Proceedings of the National Academy of Sciences*, *102*(27), 9673-9678.

Gonzalez, J. P., & Brogden, R. N. (1988). Naltrexone. *Drugs*, *35*(3), 192-213.

Guterstam, J., Jayaram-Lindström, N., Berrebi, J., Petrovic, P., Ingvar, M., Fransson, P., & Franck, J. (2018). Cue reactivity and opioid blockade in amphetamine dependence: A randomized, controlled fMRI study. *Drug and alcohol dependence*, *191*, 91-97.

Hacker, C. D., Laumann, T. O., Szrama, N. P., Baldassarre, A., Snyder, A. Z., Leuthardt, E. C., & Corbetta, M. (2013). Resting state network estimation in individual subjects. *Neuroimage*, *82*, 616-633.

Hiller, J. M., & Fan, L. Q. (1996). Laminar distribution of the multiple opioid receptors in the human cerebral cortex. *Neurochemical research*, *21*(11), 1333-1345.

Honey, G., & Bullmore, E. (2004). Human pharmacological MRI. *Trends in pharmacological sciences*, *25*(7), 366-374.

Hojjati, S. H., Ebrahimzadeh, A., Khazaee, A., Babajani-Feremi, A., & Alzheimer's Disease Neuroimaging Initiative. (2017). Predicting conversion from MCI to AD using resting-state fMRI, graph theoretical approach and SVM. *Journal of neuroscience methods*, *282*, 69-80.

Igelström, K. M., & Graziano, M. S. (2017). The inferior parietal lobule and temporoparietal junction: a network perspective. *Neuropsychologia*, *105*, 70-83.

Inagaki, T. K., Ray, L. A., Irwin, M. R., Way, B. M., & Eisenberger, N. I. (2016). Opioids and social bonding: naltrexone reduces feelings of social connection. *Social cognitive and affective neuroscience*, *11*(5), 728-735.

Jacoby, N., Bruneau, E., Koster-Hale, J., & Saxe, R. (2016). Localizing Pain Matrix and Theory of Mind networks with both verbal and non-verbal stimuli. *Neuroimage*, *126*, 39-48.

Janezic, D., Milicevic, A., Nikolic, S., & Trinajstic, N. (2015). *Graph-theoretical matrices in chemistry*. CRC Press.

Janssen, R. J., Mourão-Miranda, J., & Schnack, H. G. (2018). Making individual prognoses in psychiatry using neuroimaging and machine learning. *Biological Psychiatry: Cognitive Neuroscience and Neuroimaging*.

Jones, A. K. P., Qi, L. Y., Fujirawa, T., Luthra, S. K., Ashburner, J., Bloomfield, P., ... & Jones, T. (1991). In vivo distribution of opioid receptors in man in relation to the cortical projections of the medial and lateral pain systems measured with positron emission tomography. *Neuroscience letters*, *126*(1), 25-28.

Ravert, H. T., Bencherif, B., Madar, I., & Frost, J. J. (2004). PET imaging of opioid receptors in pain: progress and new directions. *Current pharmaceutical design*, *10*(7), 759-768.

Razi, A., Kahan, J., Rees, G., & Friston, K. J. (2015). Construct validation of a DCM for resting state fMRI. *Neuroimage*, *106*, 1-14.

Khazaee, A., Ebrahimzadeh, A., Babajani-Feremi, A., & Alzheimer's Disease Neuroimaging Initiative. (2017). Classification of patients with MCI and AD from healthy controls using directed graph measures of resting-state fMRI. *Behavioural brain research*, *322*, 339-350.

Ko, M. C., Butelman, E. R., Traynor, J. R., & Woods, J. H. (1998). Differentiation of kappa opioid agonist-induced antinociception by naltrexone apparent pA2 analysis in rhesus monkeys. *Journal of Pharmacology and Experimental Therapeutics*, *285*(2), 518-526.

Lamm, C., Decety, J., & Singer, T. (2011). Meta-analytic evidence for common and distinct neural networks associated with directly experienced pain and empathy for pain. *Neuroimage*, *54*(3), 2492-2502.

Langleben, D. D., Busch, E. L., O'Brien, C. P., & Elman, I. (2012). Depot naltrexone decreases rewarding properties of sugar in patients with opioid dependence. *Psychopharmacology*, *220*(3), 559-564.

LeCun, Y., Bengio, Y., & Hinton, G. (2015). Deep learning. *nature*, *521*(7553), 436.

Lee, M. C., Wagner, H. N., Tanada, S., Frost, J. J., Bice, A. N., & Dannals, R. F. (1988). Duration of occupancy of opiate receptors by naltrexone. *Journal of Nuclear Medicine*, *29*(7), 1207-1211.

Leech, R., & Sharp, D. J. (2013). The role of the posterior cingulate cortex in cognition and disease. *Brain*, *137*(1), 12-32.

Leppä, M., Korvenoja, A., Carlson, S., Timonen, P., Martinkauppi, S., Ahonen, J., ... & Kalso, E. (2006). Acute opioid effects on human brain as revealed by functional magnetic resonance imaging. *Neuroimage*, *31*(2), 661-669.

Leslie, R. A., & James, M. F. (2000). Pharmacological magnetic resonance imaging: a new application for functional MRI. *Trends in pharmacological sciences*, *21*(8), 314-318.

Lord, L. D., Stevner, A. B., Deco, G., & Kringelbach, M. L. (2017). Understanding principles of integration and segregation using whole-brain computational connectomics: implications for neuropsychiatric disorders. *Philosophical Transactions of the Royal Society A: Mathematical, Physical and Engineering Sciences*, *375*(2096), 20160283.

Lou, H. C., Changeux, J. P., & Rosenstand, A. (2017). Towards a cognitive neuroscience of self-awareness. *Neuroscience & Biobehavioral Reviews*, *83*, 765-773.

Lukas, S. E., Lowen, S. B., Lindsey, K. P., Conn, N., Tartarini, W., Rodolico, J., ... & Penetar, D. M. (2013). Extended-release naltrexone (XR-NTX) attenuates brain responses to alcohol cues in alcohol-dependent volunteers: a bold FMRI study. *Neuroimage*, *78*, 176-185.

Ma, N., Liu, Y., Fu, X. M., Li, N., Wang, C. X., Zhang, H., ... & Zhang, D. R. (2011). Abnormal brain default-mode network functional connectivity in drug addicts. *PloS one*, *6*(1), e16560.

Ma, X., Qiu, Y., Tian, J., Wang, J., Li, S., Zhan, W., ... & Xu, Y. (2015). Aberrant default-mode functional and structural connectivity in heroin-dependent individuals. *PLoS One*, *10*(4), e0120861.

Mallik, A., Chanda, M. L., & Levitin, D. J. (2017). Anhedonia to music and mu-opioids: Evidence from the administration of naltrexone. *Scientific reports*, *7*, 41952.

Mann, K., Vollstädt-Klein, S., Reinhard, I., Leménager, T., Fauth-Bühler, M., Hermann, D., ... & Smolka, M. N. (2014). Predicting naltrexone response in alcohol-dependent patients: the contribution of functional magnetic resonance imaging. *Alcoholism: Clinical and Experimental Research*, *38*(11), 2754-2762.

Martin-Soelch, C., Chevalley, A. F., Künig, G., Missimer, J., Magyar, S., Mino, A., ... & Leenders, K. L. (2001). Changes in reward-induced brain activation in opiate addicts. *European Journal of Neuroscience*, *14*(8), 1360-1368.

Maddock, R. J., Garrett, A. S., & Buonocore, M. H. (2003). Posterior cingulate cortex activation by emotional words: fMRI evidence from a valence decision task. *Human brain mapping*, *18*(1), 30-41.

Makovac, E., Mancini, M., Fagioli, S., Watson, D. R., Meeten, F., Rae, C. L., ... & Ottaviani, C. (2018). Network abnormalities in generalized anxiety pervade beyond the amygdala-pre-frontal cortex circuit: Insights from graph theory. *Psychiatry Research: Neuroimaging*, *281*, 107-116.

Moradi, E., Pepe, A., Gaser, C., Huttunen, H., Tohka, J., & Alzheimer's Disease Neuroimaging Initiative. (2015). Machine learning framework for early MRI-based Alzheimer's conversion prediction in MCI subjects. *Neuroimage*, 104, 398-412.

Morris, L. S., Baek, K., Tait, R., Elliott, R., Ersche, K. D., Flechais, R., ... & Passetti, F. (2018). Naltrexone ameliorates functional network abnormalities in alcohol-dependent individuals. *Addiction biology*, *23*(1), 425-436.

Murray, E., Brouwer, S., McCutcheon, R., Harmer, C. J., Cowen, P. J., & McCabe, C. (2014). Opposing neural effects of naltrexone on food reward and aversion: implications for the treatment of obesity. *Psychopharmacology*, *231*(22), 4323-4335.

Newman, M. E. (2006). Modularity and community structure in networks. *Proceedings of the national academy of sciences*, *103*(23), 8577-8582.

Nummenmaa, L., Saanijoki, T., Tuominen, L., Hirvonen, J., Tuulari, J. J., Nuutila, P., & Kalliokoski, K. (2018). μ-opioid receptor system mediates reward processing in humans. *Nature communications*, *9*(1), 1500.

Nummenmaa, L., & Tuominen, L. (2018). Opioid system and human emotions. *British journal of pharmacology*, *175*(14), 2737-2749.

Parkes, L., Fulcher, B., Yücel, M., & Fornito, A. (2018). An evaluation of the efficacy, reliability, and sensitivity of motion correction strategies for resting-state functional MRI. *NeuroImage*,171, 415-436.

Pedersen, M., Omidvarnia, A. H., Walz, J. M., & Jackson, G. D. (2015). Increased segregation of brain networks in focal epilepsy: an fMRI graph theory finding. *NeuroImage: Clinical*, *8*, 536-542.

Pedregosa, F., Varoquaux, G., Gramfort, A., Michel, V., Thirion, B., Grisel, O., ... & Vanderplas, J. (2011). Scikit-learn: Machine learning in Python. *Journal of machine learning research*, *12*(Oct), 2825-2830.

Pereira, F., Mitchell, T., & Botvinick, M. (2009). Machine learning classifiers and fMRI: a tutorial overview. *Neuroimage*, *45*(1), 199-209.

Polunina, A. G., & Bryun, E. A. (2013). Neuropsychological Functions of μ-and δ-Opioid Systems. *ISRN Addiction*, *2013*.

Pomares, F. B., Faillenot, I., Barral, F. G., & Peyron, R. (2013). The 'where'and the 'when'of the BOLD response to pain in the insular cortex. Discussion on amplitudes and latencies. *Neuroimage*, *64*, 466-475.

Power, J. D., Cohen, A. L., Nelson, S. M., Wig, G. S., Barnes, K. A., Church, J. A., ... & Petersen, S. E. (2011). Functional network organization of the human brain. *Neuron*, *72*(4), 665-678.

Power, J. D., Mitra, A., Laumann, T. O., Snyder, A. Z., Schlaggar, B. L., & Petersen, S. E. (2014). Methods to detect, characterize, and remove motion artifact in resting state fMRI. *Neuroimage*, *84*, 320-341.

Power, J. D., Schlaggar, B. L., & Petersen, S. E. (2015). Recent progress and outstanding issues in motion correction in resting state fMRI. *Neuroimage*, *105*, 536-551.

Quirion, R., & Pilapil, C. (1991). Distribution of multiple opioid receptors in the human brain. In *Receptors in the human nervous system* (pp. 103-121). Academic Press.

Raichle, M. E. (2015). The brain's default mode network. *Annual review of neuroscience*, *38*, 433-447.

Rütgen, M., Seidel, E. M., Silani, G., Riečanský, I., Hummer, A., Windischberger, C., ... & Lamm, C. (2015). Placebo analgesia and its opioidergic regulation suggest that empathy for pain is grounded in self pain. *Proceedings of the National Academy of Sciences*, *112*(41), E5638-E5646.

Rütgen, M., Seidel, E. M., Pletti, C., Riečanský, I., Gartus, A., Eisenegger, C., & Lamm, C. (2018). Psychopharmacological modulation of event-related potentials suggests that first-hand pain and empathy for pain rely on similar opioidergic processes. *Neuropsychologia*, *116*, 5-14.

Sato, J. R., Biazoli Jr, C. E., Salum, G. A., Gadelha, A., Crossley, N., Vieira, G., ... & Amaro Jr, E. (2018). Association between abnormal brain functional connectivity in children and psychopathology: A study based on graph theory and machine learning. *The World Journal of Biological Psychiatry*, *19*(2), 119-129.

Sacchet, M. D., Prasad, G., Foland-Ross, L. C., Thompson, P. M., & Gotlib, I. H. (2015). Support vector machine classification of major depressive disorder using diffusion-weighted neuroimaging and graph theory. *Frontiers in psychiatry*, *6*, 21.

Satterthwaite, T. D., Elliott, M. A., Gerraty, R. T., Ruparel, K., Loughead, J., Calkins, M. E., ... & Wolf, D. H. (2013). An improved framework for confound regression and filtering for control of motion artifact in the preprocessing of resting-state functional connectivity data. *Neuroimage*, *64*, 240-256.

Schadrack, J., Willoch, F., Platzer, S., Bartenstein, P., Mahal, B., Dworzak, D., ... & Tölle, T. R. (1999). Opioid receptors in the human cerebellum: evidence from [11C] diprenorphine PET, mRNA expression and autoradiography. *Neuroreport*, *10*(3), 619-624.

Smith, R., Lane, R. D., Alkozei, A., Bao, J., Smith, C., Sanova, A., ... & Killgore, W. D. (2018). The role of medial prefrontal cortex in the working memory maintenance of one's own emotional responses. *Scientific reports*, *8*(1), 3460.

Smith, J. S., Zubieta, J. K., Price, J. C., Flesher, J. E., Madar, I., Lever, J. R., ... & Frost, J. J. (1999). Quantification of δ-opioid receptors in human brain with N1′-([11C] methyl) naltrindole and positron emission tomography. *Journal of Cerebral Blood Flow & Metabolism*, *19*(9), 956-966.

Sprenger, T., Berthele, A., Platzer, S., Boecker, H., & Tölle, T. R. (2005). What to learn from in vivo opioidergic brain imaging?. *European Journal of Pain*, *9*(2), 117-121.

Sporns, O., & Zwi, J. D. (2004). The small world of the cerebral cortex. *Neuroinformatics*, *2*(2), 145-162.

Sporns, O., Chialvo, D. R., Kaiser, M., & Hilgetag, C. C. (2004). Organization, development and function of complex brain networks. *Trends in cognitive sciences*, *8*(9), 418-425.

Stephan, K. E., Penny, W. D., Moran, R. J., den Ouden, H. E., Daunizeau, J., & Friston, K. J. (2010). Ten simple rules for dynamic causal modeling. *Neuroimage*, *49*(4), 3099-3109.

Trenn, S. (2008). Multilayer perceptrons: Approximation order and necessary number of hidden units. *IEEE Transactions on Neural Networks*, *19*(5), 836-844.

Van Der Walt, S., Colbert, S. C., & Varoquaux, G. (2011). The NumPy array: a structure for efficient numerical computation. *Computing in Science & Engineering*, *13*(2), 22.

Van Dijk, K. R., Sabuncu, M. R., & Buckner, R. L. (2012). The influence of head motion on intrinsic functional connectivity MRI. *Neuroimage*, *59*(1), 431-438.

Verebey, K., Volavka, J., Mule, S. J., & Resnick, R. B. (1976). Naltrexone: disposition, metabolism, and effects after acute and chronic dosing. *Clinical Pharmacology & Therapeutics*, *20*(3), 315-328.

Vieira, S., Pinaya, W. H., & Mechelli, A. (2017). Using deep learning to investigate the neuroimaging correlates of psychiatric and neurological disorders: Methods and applications. *Neuroscience & Biobehavioral Reviews*, *74*, 58-75.

Vogt, K. M., Becker, C. J., Wasan, A. D., & Ibinson, J. W. (2016). Human posterior insula functional connectivity differs between electrical pain and the resting state. *Brain connectivity*, *6*(10), 786-794.

Wager, T. D., Rilling, J. K., Smith, E. E., Sokolik, A., Casey, K. L., Davidson, R. J., ... & Cohen, J. D. (2004). Placebo-induced changes in FMRI in the anticipation and experience of pain. *Science*, *303*(5661), 1162-1167.
Watts, D. J., & Strogatz, S. H. (1998). Collective dynamics of 'small-world'networks. *nature*, *393*(6684), 440.

Walter, M., Alizadeh, S., Jamalabadi, H., Lueken, U., Dannlowski, U., Walter, H., ... & Hahn, T. (2018). Translational machine learning for psychiatric neuroimaging. *Progress in Neuro-Psychopharmacology and Biological Psychiatry*.

Wang, J., Wang, L., Zang, Y., Yang, H., Tang, H., Gong, Q., ... & He, Y. (2009). Parcellation-dependent small-world brain functional networks: A resting-state fMRI study. *Human brain mapping*, *30*(5), 1511-1523.

Wang, A. L., Elman, I., Lowen, S. B., Blady, S. J., Lynch, K. G., Hyatt, J. M., ... & Langleben, D. D. (2015). Neural correlates of adherence to extended-release naltrexone pharmacotherapy in heroin dependence. *Translational psychiatry*, *5*(3), e531.

Wang, J. H., Zuo, X. N., Gohel, S., Milham, M. P., Biswal, B. B., & He, Y. (2011). Graph theoretical analysis of functional brain networks: test-retest evaluation on short-and long-term resting-state functional MRI data. *PloS one*, *6*(7), e21976.

Wang, J., Wang, X., Xia, M., Liao, X., Evans, A., & He, Y. (2015). GRETNA: a graph theoretical network analysis toolbox for imaging connectomics. *Frontiers in human neuroscience*, *9*, 386.

Wardle, M. C., Bershad, A. K., & de Wit, H. (2016). Naltrexone alters the processing of social and emotional stimuli in healthy adults. *Social neuroscience*, *11*(6), 579-591.

Weerts, E. M., Kim, Y. K., Wand, G. S., Dannals, R. F., Lee, J. S., Frost, J. J., & McCaul, M. E. (2008). Differences in δ-and μ-opioid receptor blockade measured by positron emission tomography in naltrexone-treated recently abstinent alcohol-dependent subjects. *Neuropsychopharmacology*, *33*(3), 653.

Werner, M. U., Pereira, M. P., Andersen, L. P. H., & Dahl, J. B. (2015). Endogenous opioid antagonism in physiological experimental pain models: a systematic review. *PloS one*, *10*(6), e0125887.

Wittmann, M., Leland, D. S., & Paulus, M. P. (2007). Time and decision making: differential contribution of the posterior insular cortex and the striatum during a delay discounting task. *Experimental Brain Research*, *179*(4), 643-653.

Xia, M., Wang, J., & He, Y. (2013). BrainNet Viewer: a network visualization tool for human brain connectomics. *PloS one*, *8*(7), e68910.

Zalesky, A., Fornito, A., & Bullmore, E. T. (2010). Network-based statistic: identifying differences in brain networks. *Neuroimage*, *53*(4), 1197-1207.

Zhang, W., Chien, J., Yong, J., & Kuang, R. (2017). Network-based machine learning and graph theory algorithms for precision oncology. *NPJ precision oncology*, *1*(1), 25.

Zubieta, J. K., Ketter, T. A., Bueller, J. A., Xu, Y., Kilbourn, M. R., Young, E. A., & Koeppe, R. A. (2003). Regulation of human affective responses by anterior cingulate and limbic μ-opioid neurotransmission. *Archives of general psychiatry*, *60*(11), 1145-1153.

Appendix

A. Abstract

Resting state functional magnetic resonance imaging (rs-fMRI) has gained substantial momentum within the field of the neurosciences for its ability to elucidate spontaneous neuronal fluctuations in the brain during rest. Amongst others, this methods has largely contributed to a proliferated understanding of aberrations in neuronal connectivity in healthy and clinical populations alike. Conjoined with the power of machine learning (ML) approaches, it has by these means become increasingly popular to employ rs-fMRI data for investigating the influence of neuropharmacological compounds, such as Naltrexone (NTX), on neuronal connectivity.

NTX, a powerful non-selective opioid receptor antagonist, is a commonly administered treatment in substance use disorders, but has also been drawn on to manipulate neuronal activity related to reward or empathy for pain in healthy study populations in experimental paradigms of the social, cognitive and affective neurosciences. However, partially due to rather small sample sizes and a limitation of fMRI analysis to mostly univariate approaches, past research has failed to yield converging evidence on the neuronal effects of NTX. Thus, to date, neuronal connectivity aberrations induced by NTX, especially in healthy subgroups, remain largely unclear.

With the aim to bridge limitations of previous research and to do justice to the substantial importance of a proliferated understanding of NTX-induced neuronal connectivity aberrations for both neuroscientific or clinical research, as well as for clinical application, the present study intends to elucidate NTX-related neuronal connectivity modulations in healthy individuals at rest by exploiting joined graph theoretical, functional and effective connectivity analyses as well as ML. This exploratory multi-methodological account thereby aims to investigate key areas eligible for empathy and reward-related processes, encompassing the insula, cingulate, medial and ventrolateral prefrontal cortex.

By these means, we are able demonstrate that the intake of NTX entails neuronal aberrations in functional and effective connectivity, as well as changes on a graph theoretical level in regions involved in affective coding, empathy judgement, proprioceptive integration and reward. Taken together, our study lays grounds for an advanced understanding of the mechanism of action of NTX in healthy individuals and, in this vein, will largely benefit future neuroscientific research as well as clinical practice.

B. Zusammenfassung

Die Methode der funktionellen Magnetresonanztomographie im Ruhezustand (rs-fMRI), die es ermöglicht, spontane neuronale Fluktuationen im Gehirn im Ruhezustand zu messen, hat in den letzten Jahren in den Neurowissenschaften an Bedeutung gewonnen. Unter anderem hat rs-fMRI zu einem vertieften Verständnis neuronaler Modulationen funktioneller Konnektivität, sowohl in gesunden als auch klinischen Populationen beigetragen. Zusammen mit dem Potential von maschinellem Lernen (ML) wurde es immer populärer, mithilfe von rs-fMRI den Einfluss neuropharmakologisch aktiver Substanzen, wie beispielsweise Naltrexon (NTX), auf neuronale Konnektivität zu messen.

NTX, ein hochwirksamer non-selektiver Opioid Rezeptor Antagonist, der häufig Verwendung in der Behandlung von Abhängigkeitserkrankungen findet, wurde in den sozialen, kognitiven und affektiven, Neurowissenschaften auch immer wieder für die Manipulation neuronaler Aktivität im Zusammenhang mit Belohnung oder Empathie für Schmerz in gesunden als auch klinischen Populationen herangezogen. Jedoch war es vergangenen Studien, teilweise aufgrund von zu geringer Stichprobengrößen und der methodischen Beschränkung auf univariate fMRI Analyseverfahren, noch nicht möglich konvergierende Ergebnisse hinsichtlich der NTX-induzierten neuronalen Konnektivitätsveränderungen hervorzubringen. Daher sind die Mechanismen NTX-induzierter neuronaler Konnektivitätsveränderungen bisherig noch großteils unverstanden.

Unter Verwendung graph-theoretischer, funktioneller und effektiver Konnektivitätsanalysen und aktueller Methoden des ML (tiefe neuronale Netze) zielen wir darauf ab, mit unserem kombinierten methodischen Ansatz Limitationen vorheriger Studien zu überwinden und zu einem vertieften Verständnis von neuronalen Effekten von NTX in gesunden Personen beizutragen.

Mit diesem explorativen, multi-methdologischen Ansatz streben wir neue Erkenntnisse bezüglich der neuronalen modulatorischen Effekte von NTX auf Areale wie die insula, den cingulären cortex, sowie präfrontale Areale, die in Empathie und Belohnungsprozesse involviert sind, an. Auf Grundlage unserer Untersuchung können wir zeigen, dass die Administration von NTX in gesunden ProbandInnen zu neuronalen Modulationen in Arealen, die in affektiven Prozessen, Empathie, propriozeptiver Integration und Belohnung involviert sind, führt. Zusammengefasst leistet unsere Studie einen wichtigen Beitrag zum fortgeschrittenen Verständnis der neuronalen Wirkmechanismen von NTX in gesunden ProbandInnen, was sowohl zukünftiger neurowissenschaftlicher als auch klinischer Forschung zugute kommen wird.

C. List of Tables

D. List of Figures

E. Supplementary Information

Abbreviations

TR= Time of repition
TE= Echo Time
FOV= Field of View

Abbreviations of brain regions

Abbreviation	Region
CC	Cingulate Cortex
aCC	Anterior Cingulate Cortex
pCC	Posterior Cingulate Cortex
INS	Insula
aINS	Anterior Insula
mINS	Medial Insula
pINS	Posterior Insula
AG	Angular Gyrus
FG	Fusiform Gyrus
BG	Basal Ganglia
mPFC	Medial Prefrontal Cortex
SupPFC	Superior Prefrontal Cortex
TPJ	Temporo Parietal Junction
PFC	Prefrontal Cortex
vaPFC	Ventral anterior Prefrontal Cortex
dlPFC	Dorsolateral Prefrontal Cortex
dFC	Dorsal Frontal Cortex
vFC	Ventral Frontal Cortex
vlFC	Ventro lateral Prefrontal Cortex
PrecGyr	Precentral Gyrus
VAC	Visual Association Cortex
SecVC	Secondary Visual Cortex
SecSMC	Secondary Motor Cortex
STC	Superior Temporal Cortex
TC	Temporal Cortex
MTG	Medial Temporal Gyrus
PrimSC	Primary Sensory Cortex
IPL	Inferior Parietal Lobule
IPS	Inferior Parietal Sulcus
SMA	Supplemantary Motor Area
Precun	Precuneus
IT	Inferior Temporal Cortex
Sensory Cort	Sensory Cortex
Post Occipit	Post Occipital Cortex
Post Pariet	Post Parietal Cortex
FusGyr	Fusiform Gyrus
InfCereb	Inferior Cerebellum
MedCereb	Medial Cerebellum

Exclusion criteria. Criteria from the clinical screening prior to the testing sessions:

- Intolerance against naltrexone, naloxone and opiates
- Disease of the central nervous system, brain trauma (current or in the personal anamnesis)
- Psychological disorder (current or in the personal anamnesis)
- Internal diseases (current, the former were further assessed)
- Body mass index (BMI) beyond the standard limits (< 18.5 or > 30)
- Other exclusion criteria referring to fMRI guidelines (metal items etc.)

fMRI safety criteria. The following criteria were assessed (if the answer was yes, more information was requested).

- previous MRI examination
- prior head, heart or vascular system surgery
- presence of a pacemaker
- presence of any other electronic, magnetic or mechanic implants
- presence of surgical implants
- presence of metallic prostheses
- presence other metallic parts or splinters in the body
- previous work with metal without wearing eye protection
- presence of medical patches
- need for some kind of hearing aid
- presence of braces/a retainer/dental prostheses
- need for glasses or contact lenses
- usage of colored contact lenses
- presence of one or more tattoos
- presence of permanent make-up
- presence of one or more piercings
- fear of closed or narrowed spaces/presence of claustrophobia
- sensibility to noise/hardness of hearing
- recent/current intake of any medication
- presence of any illness
- for women: possible pregnancy
- for women: presence of an intrauterine device

Table 5 Functional Connectivity Analysis of Mean Group Adjacency Matrices

ROI	MNI			NTX		CON		*t*	*p*
	x	y	z	M	SEM	M	SEM		
aCC	9	39	20	0.04	0.10	0.03	0.09	2.92	0.03
pCC	1	-26	31	0.03	0.06	0.04	0.08	-4-14	< .0001
	10	-55	17	0.04	0.14	0.05	0.15	-2.70	0.05
	-4	-31	-4	0.08	0.10	0.06	0.10	2.70	0.05
FusGyr	28	-37	-15	0.06	0.11	0.06	0.08	-3.38	0.001
Occipital	28	-42	-11	0.06	0.09	0.03	0.06	2.72	0.05
	-42	-76	26	0.06	0.10	0.07	0.11	-4.25	<.0001
IPS	-36	-69	40	0.06	0.07	0.05	0.09	-3.56	0.01
	-32	-58	46	0.06	0.11	0.03	0.07	3.68	0.01
vaPFC	42	48	-3	0.08	0.10	0.02	0.09	4.79	<.0001
dlPFC	46	28	31	0.04	0.08	0.05	0.09	-3.63	0.01
dFC	-42	7	36	0.06	0.09	0.01	0.09	2.91	0.03
vFC	43	1	12	0.07	0.13	0.03	0.10	4.63	<.0001
vlPFC	36	39	-15	0.07	0.10	0.04	0.07	3.52	0.01
aINS	38	21	-1	0.07	0.11	0.03	0.08	4.09	<.0001
BG	-6	17	34	0.06	0.10	0.02	0.09	3.63	0.01
	14	6	7	0.03	0.07	0.02	0.08	-2.70	0.05
Thalamus	-12	-12	6	0.04	0.15	0.05	0.15	-2.89	0.03
	11	-12	6	0.09	0.04	0.5	0.10	-3.41	0.01
Temporal	46	-62	5	0.06	0.07	0.06	0.09	-3.22	0.01
Occipital	-29	-75	28	0.07	0.06	0.07	0.08	-3.48	0.01
	-16	-76	33	0.05	0.07	0.05	0.09	-4.51	<.0001
	33	-81	-2	0.07	0.10	0.04	0.08	2.77	0.04
Cerebellum	-37	-54	-37	0.03	0.06	0.06	0.08	-3.87	<.0001
	-25	-60	-34	0.08	0.12	0.05	0.09	3.52	0.01
	-16	-64	-21	0.02	0.07	0.04	0.08	-3.38	0.01
	-34	-67	-29	0.09	0.09	0.06	0.10	3.10	0.02

Note. Display of group wise functional connectivity analysis. Averaged connectivity matrices were thresholded with 0.15% and binarized. Subsequently, a paired t-test (FDR-corrected) was conducted.

Table 6 Paired t-test of Nodal Local Efficiency (FDR-corrected)

ROI	Side	MNI			*t*	*p*
		x	y	z		
SMA	L	-42	7	36	2.71	<.05
vlPFC	R	58	11	14	3.30	<.05
	R	46	39	-15	5.17	<.001
Thalamus	R	11	-12	6	-4.77	<.001
Post Occipit	R	33	-81	-2	4.21	<.01
	L	-5	-80	9	-4.49	<.001
TC	R	46	-62	5	6.04	<.0001
	R	39	-71	13	-4.83	<.001
	R	19	-66	-1	3.10	<.05
STG	L	-59	-47	11	3.80	<.05
	R	51	-30	5	-4.65	<.001
SupTemporal	R	42	-46	21	-4.37	<.01
SMA	R	23	33	47	5.30	<.001
Precun	R	8	-40	50	-3.15	<.05
	R	11	-68	42	-5.44	<.001
	L	-6	-56	29	3.40	<.01
	R	9	-43	25	-2.83	<.05
PrecGyr	R	44	-11	38	4.57	<.001
	L	-44	-6	49	4.21	<.01
pINS	R	42	-24	17	-3.04	<.05
PrimSC	L	-47	-18	50	4.05	<.01
PMA	L	-26	-8	54	4.61	<.001
Occipital	L	-44	-63	-7	3.04	<.05
	L	-28	-42	-11	-3.67	<.01
	R	36	-60	-8	2.73	<.05
SPL	L	-9	-72	41	-3.43	<.05
AG	R	29	-73	29	-3.03	<.05
STG	R	52	-15	-13	6.34	<.0001
InfCereb	R	18	-81	-33	-2.75	<.05
	L	-21	-79	-33	-2.96	<.05
BG	R	11	-24	2	-3.23	<.05
AG	L	-48	-63	35	-3.29	<.05
IPS	L	-32	-58	46	2.86	<.05
	L	-36	-69	40	-3.36	<.05
	L	-53	-50	39	-2.76	<.05

Note. Display of statistical ROI wise analysis of the Nodal Local Efficiency (AUC).

Table 7 Statistical Analysis of Nodal Cluster Coefficient (FDR-corrected)

ROI	Side	MNI			*t*	*p*
		x	y	z		
CC	L	-1	28	40	-3.29	<.001
	L	-2	30	27	2.58	<.05
pCC	R	1	-26	31	3.75	<.01
	L	-5	-43	25	-3.01	<.01
	R	10	-55	17	3.90	<.01
	L	-11	-58	17	4.30	<.001
aINS	R	38	21	-1	3.76	<.0015
mINS	R	32	-12	2	-3.76	<.0015
pINS	L	-30	-28	9	-8.64	<.0001
	R	42	-24	17	-5.80	<.0001
Precun	R	9	-43	25	-3.57	<.01
	L	-6	-56	29	5.76	<.0001
	R	11	-68	42	-8.28	<.0001
	R	8	-40	50	-2.89	<.05
AG	L	-41	-40	42	30.40	<.05
	R	54	-44	43	28.25	<.05
	L	-48	-47	49	-26.40	<.01
	L	-53	-50	39	-21.13	<.01
	R	44	-52	47	-19.34	<.01
IPS	L	-36	-69	40	-5.54	<.01
	L	-32	-58	45	-5.08	< .0001
SMA		0	-1	52	-4.99	< .0001
Pre SMA	R	10	5	51	-2.81	<.05
TPJ	L	-52	-63	15	2.79	<.0.05
PFC	L	-25	51	27	5.24	< .0001
	R	27	49	26	-3.78	<.001
	R	44	8	34	5.10	<.0001
	L	-42	7	36	24.29	<.0001
	L	-44	27	33	2.41	<.05
	R	46	28	31	-3.60	<.05
	R	58	11	14	4.47	<.001
	R	53	-3	32	-4.41	<.001
	R	43	1	12	-3.19	<.01
	L	-43	47	2	2.48	<.05
	R	46	39	-15	8.39	<.0001
	R	6	64	3	4.80	<.0001
	L	-11	45	17	-2.81	<.05
Mid PFC		0	51	32	5.12	<.0001
Sup PFC	R	23	33	47	9.68	<.0001
	L	-16	28	54	5.37	<.0001
IT	R	52	-15	-13	9.05	<.0001
PrecGyrus	R	58	-3	17	-3.11	<.01

	L	-44	-6	49	4.56	<.001
	R	44	-11	38	5.01	<.0001
	L	-54	-22	22	3.63	<.01
FG	R	54	-31	-18	-4.35	<.001
Inf Cereb	L	-21	-79	-33	-5.10	<.001
	L	-6	-79	-33	-3.55	<.001
	R	18	-81	-33	-3.75	<.01
Med Cereb	L	-6	-60	-15	-2.75	<.05
	L	-16	-64	-21	2.70	<.05
AG	L	-48	-63	35	-6.50	<.0001
	L	-30	-14	1	-5.09	<.0001
	L	-36	-12	15	-4.27	<.001
Occipital	R	19	-66	-1	4.99	<.0001
	R	17	-68	20	-3.09	<.01
	R	39	-71	13	-5.86	<.0001
	R	29	-71	13	-4.19	<.001
	R	9	-76	14	2.52	<.05
	R	36	-60	-8	7.41	<.0001
	L	-28	-42	-11	-6.26	<.0001
	L	-9	-72	41	-4.44	<.01
Post Occip	L	-5	-80	9	-7.11	<.0001
	R	29	-81	14	-4.38	<.001
	R	33	-81	-2	-5.22	<.0001
	L	-44	-63	-7	7.18	<.0001
Parietal	R	58	-41	20	-5.53	<.0001
	R	41	-23	55	-4.10	<.001
	R	18	-27	62	-4.73	<.001
	L	-38	-27	60	-3.14	<.01
	L	-26	-8	54	4.96	<.0001
	L	-47	-18	50	3.24	<.01
	L	-55	-22	38	3.76	<.01
Post Pariet		-41	-31	48	-2.56	<.05
STC	R	42	-46	21	-3.37	<.01
TC	R	51	-30	5	-3.19	<.01
	R	43	-43	8	-2.85	<.05
	L	-59	-47	11	5.77	<.0001
	R	59	-13	8	-5.42	<.0001
	L	-41	-37	16	-3.75	<.01
	R	46	-62	5	9.66	<.0001
BG	R	14	6	7	-3.46	<.01
	R	11	-24	2	-5.26	<.0001

Note. Display of statistical ROI wise analysis of the Nodal Cluster Coefficient (AUC).

Table 8 Statistical analysis of Nodal Efficiency (FDR-corrected)

ROI	Side	MNI			*p*	*t*
		x	y	z		
MFG	R	6	64	3	-4.41	<.001
	R	39	42	16	3.80	<.05
	L	-52	28	17	-3.35	<.01
	R	40	36	29	2.83	<.05
vlPFC	R	46	39	-15	-5.34	<.0001
	L	-25	51	27	-3.81	<.01
vmPFC	R	1	-26	31	-4.00	<.01
	L	-6	50	-1	2.64	<.05
PMC	R	43	1	12	4.04	<.01
	R	53	-3	32	5.35	<.0001
	R	46	-20	45	-2.53	<.05
	R	41	-23	55	3.01	<.05
SMA	L	-16	29	54	-6.73	<.0001
	R	23	33	47	-5.18	<.001
mPFC		0	51	32	-3.39	<.01
FusGyr	R	28	-37	-15	-3.64	<.01
AG	L	-41	-47	29	-3.47	<.05
	L	-48	-63	35	4.29	<.01
	L	-38	-15	59	3.96	<.01
TPJ	L	-52	-63	15	-3.12	<.05
IPS	R	32	-59	41	-3.26	<.01
	L	-36	-69	40	2.85	<.05
IPL	L	-41	-40	42	-2.66	<.05
	L	-59	-47	11	-3.52	<.01
	L	-55	-22	38	-5.11	<.001
	L	-55	-44	30	5.28	<.0001
PreGyr	R	58	-3	17	3.00	<.05
SecSMC	L	-35	-46	48	-4.14	<.01
Post Occipital	L	-4	-94	12	3.62	<.01
Occipital	L	-44	-63	-7	-7.12	<.0001
SupTemporal	R	59	-13	8	4.72	<.001
	R	42	-46	21	-6.52	<.0001
InfTemporal	R	52	-15	13	-2.76	<.05
TC	R	43	-43	8	-3.85	<.01
	L	-59	-47	11	5.76	<.0001
	R	59	-13	8	-5.42	<.0001
	L	-41	-37	16	-3.75	<.01
	R	46	-62	5	-4.33	<.001
Thalamus	L	-12	-3	13	4.16	<.01
MTG	R	43	-43	8	4.82	<.001
Precun	R	8	-40	50	2.86	<.05
	R	11	-68	42	3.53	<.05

	L	-6	-56	29	3.58	<.01
	R	5	-50	33	2.70	<.05
	L	-3	-38	45	3.37	<.01
pINS	R	42	-94	12	3.06	<.05
mINS	L	-36	-12	15	3.68	<.01
aCC	L	-1	28	40	4.12	<.01
pCC	L	-11	-58	17	-5.30	<.0001
	R	10	-55	17	-4.13	<.01
	R	1	-26	31	-3.40	<.01
Sensory Cort	L	-47	-18	50	5.60	<.0001
	R	48	-41	20	3.29	<.01
Occipital	R	36	-60	-8	-7.68	<.0001
	R	19	-66	-1	-2.76	<.05
LatCerebellum	L	-24	-54	-21	3.32	<.01
	L	-28	-44	-25	5.46	<.0001
InfCerebellum	L	-37	-54	-37	3.44	<.01

Note. Display of statistical ROI wise analysis of Nodal Efficiency (AUC).

Table 9 Network Based Statistics Results

NBS Results							
Network 1							***p* < .01**
	MNI			**MNI**			***t***
	x	**y**	**z**	**x**	**y**	**y**	
Prcn > Thal	11	-68	42	11	-12	6	3.64
Prcn>AG	11	-68	42	-41	-47	29	3.78
pCC > AG	-8	-41	3	-41	-47	29	3.80
mINS>AG	-30	-14	1	-41	-47	29	4.00
mINS>PrecGyr	-30	-14	1	58	-3	17	3.62
mINS>pINS	-30	-14	1	42	-24	17	3.91
Thal>PrecGyr	-12	-12	6	-54	-9	23	3.61
Thal>pINS	-12	-12	6	42	-24	17	4.31
Thal > PrecGyr	-12	-12	6	58	-3	17	4.76
Thal>Occipital	11	-12	6	-29	-75	28	3.58
IPS > AG	32	-59	41	-41	-47	29	3.69
vmPFC>pINS	9	51	16	42	-24	17	3.52
BG > PrecGyr	-20	6	7	58	-3	17	5.50
BG>pINS	-20	6	7	42	-24	17	3.76
PrecGyr>pINS	58	-3	17	42	-24	17	3.86
Network 2							***p* < .01**
vmPFC>dlPFC	-11	45	17	46	28	31	3.82
dlPFC>dlPFC	40	36	29	46	28	31	3.65
FG>pOccipit	28	-37	-15	-29	-88	8	3.58
Occipit>Occipit	29	-81	14	-29	-88	8	3.59
Occipit>medCereb	29	-81	14	-6	-60	-15	4.76
Occpit>medCereb	29	-81	14	-6	-60	-15	3.65
Occipit>medCereb	-29	-88	8	-11	-72	-14	3.71
vmPFC>medCereb	-11	45	17	-11	-72	-14	3.61
dlPFC>medCereb	40	36	29	-11	-72	-14	4.34
dlPFC>medCereb	46	28	31	-11	-72	-14	3.85
BG>medCereb	-6	17	34	-11	-72	-14	3.60
Occipit > Inf Cereb	29	-81	14	32	-61	-31	3.58
Network 3							***p* < .02**
supFrontal>dlPFC	23	33	47	-44	27	33	4.04
supFrontal>mFC	23	33	47	0	15	45	3.81
supFrontal>preSMA	23	33	47	10	5	51	3.72
dlPFC > mFC	-44	27	33	0	15	45	3.53
dFC>preSMA	-42	7	36	10	5	51	3.63
dFC>PrecGyr	-42	7	36	46	-8	24	4.10
dFC>Parietal	-42	7	36	-47	-12	36	3.94
preSMA>SMA	10	5	51	0	-1	52	4.54
Parietal> Parietal	-47	-12	36	-55	-22	38	3.85
Network 4							***p* < .003**
pCC>AG	-5	-43	25	51	-59	34	4.31
pCC>mINS	-5	-43	25	32	-12	2	3.76
pCC>Temp	-5	-43	25	59	-13	8	3.84
pCC>Occipital	-5	-43	25	15	-77	32	3.60
pCC>Occipital	-4	-31	-4	15	-77	32	3.59
aINS>pINS	-36	18	2	-30	-28	9	3.52
aINS>vFC	-36	18	2	43	1	12	4.46
mINS>pINS	37	-2	-3	42	-24	17	3.54
pINS>Parietal	-30	-28	9	58	-41	20	4.85
pINS>supTemp	-30	-28	9	42	-46	21	4.22
pINS>Temp	-30	-28	9	59	-13	8	3.60

vFC>Parietal	-48	6	1	58	-41	20	3.72
AG>AG	51	-59	34	-48	-63	35	3.66
AG>vFC	-48	-63	35	-48	6	1	4.17
AG>mINS	51	-59	34	-30	-28	9	4.04
AG>pINS	-48	-63	35	-30	-28	9	4.06
AG>Parietal	-48	-63	35	58	-41	20	4.86
AG>supTemp	51	-59	34	42	-46	21	4.37
AG>supTemp	-48	-63	35	42	-46	21	4.52
Parietal>supTemp	58	-41	20	42	-46	21	4.07
Precun>Temp	5	-50	33	59	-13	8	5.26
Precun>PrecGyr	5	-50	33	-54	-22	22	4.59
Temp>PrecGyr	59	-13	8	-54	-22	22	3.58

Table 9. Display of NBS statistics. The sign “>” indicates the projection from one node to another node.

Table 10 Exploratory whole-brain fMRI analysis

Cluster Level				Peak Level							
FWE	FDR		u.c.	FWE	FDR	u.c.			MNI		
p	q	k	p	p	q	p	T	Z	x	y	z
0.000	0.000	93	0.000	0.000	0.000	0.000	11.89	7.53	2	53	35
0.000	0.000	72	0.000	0.000	0.000	0.000	10.86	7.19	0	-36	45
				0.001	0.077	0.000	7.46	5.77	-3	-44	48
0.000	0.000	10	0.000	0.000	0.013	0.000	8.42	6.22	0	-65	-21
0.000	0.000	11	0.000	0.000	0.013	0.000	8.39	6.21	-47	2	-5
0.000	0.000	50	0.000	0.000	0.014	0.000	8.36	6.19	12	-39	53
0.000	0.000	80	0.000	0.000	0.015	0.000	8.32	6.18	23	36	48
				0.001	0.059	0.000	7.60	5.84	29	29	47
0.000	0.000	37	0.000	0.000	0.017	0.000	8.25	6.14	-5	-63	-18
0.000	0.000	33	0.000	0.000	0.022	0.000	8.11	6.08	0	0	54
0.000	0.000	5	0.01	0.000	0.028	0.000	8	6.03	3	-53	35
0.000	0.000	35	0.00	0.000	0.029	0.000	7.98	6.02	21	-26	62
0.000	0.000	21	0.00	0.000	0.032	0.000	7.93	5.99	-26	-27	63
0.000	0.000	22	0.00	0.000	0.033	0.000	7.91	5.98	-26	-35	62
0.000	0.000	55	0.00	0.001	0.051	0.000	7.68	5.87	-54	-23	9
0.000	0.000	19	0.00	0.001	0.051	0.000	7.68	5.87	2	-26	32
0.000	0.000	17	0.00	0.001	0.055	0.000	7.65	5.86	-33	-57	41
0.012	0.099	1	0.00	0.002	0.104	0.000	7.30	5.68	27	57	14
0.000	0.000	15	0.00	0.002	0.109	0.000	7.28	5.67	57	-17	8
0.000	0.000	17	0.00	0.002	0.111	0.000	7.27	5.67	2	12	48
0.001	0.032	3	0.008	0.002	0.114	0.000	7.25	5.66	-39	-45	44
0.001	0.002	7	0.000	0.002	0.118	0.000	7.23	5.65	27	48	29
0.003	0.063	2	0.025	0.025	0.127	0.000	7.20	5.63	-33	-29	6
0.001	0.032	3	0.008	0.002	0.128	0.000	7.19	5.63	-56	-23	35
0.012	0.099	1	0.099	0.002	0.129	0.000	7.19	5.62	-12	33	53
0.000	0.000	9	0.000	0.003	0.142	0.000	7.13	5.59	41	21	36
0.003	0.063	2	0.025	0.003	0.158	0.000	7.07	5.56	41	-24	14
0.000	0.015	4	0.003	0.003	0.158	0.000	7.07	5.56	-38	-24	57
0.001	0.032	3	0.008	0.003	0.165	0.000	7.05	5.55	-8	-8	12
0.001	0.032	3	0.008	0.003	0.166	0.000	7.05	5.55	-53	-33	15
0.001	0.032	3	0.008	0.003	0.166	0.000	7.05	5.55	-56	-38	15
0.000	0.000	15	0.000	0.004	0.171	0.000	7.04	5.55	8	-54	30
0.000	0.003	6	0.000	0.004	0.179	0.000	7.01	5.53	-53	-24	39
0.003	0.063	2	0.025	0.004	0.186	0.000	7.00	5.52	2	30	42
0.012	0.099	1	0.099	0.006	0.235	0.000	6.88	5.46	-38	-20	59
0.000	0.000	10	0.000	0.006	0.241	0.000	6.86	5.45	-33	-24	8
0.001	0.032	3	0.008	0.006	0.244	0.000	6.86	5.45	-57	-14	5
0.012	0.099	1	0.099	0.008	0.281	0.000	6.79	5.41	-39	-12	57
0.000	0.002	7	0.000	0.008	0.284	0.000	6.78	5.41	42	-29	15
0.003	0.063	2	0.025	0.008	0.301	0.000	6.75	5.39	-44	-11	50
0.012	0.099	1	0.099	0.09	0.319	0.000	6.72	5.38	3	-56	33
0.000	0.002	7	0.000	0.09	0.319	0.000	6.72	5.38	41	36	26
0.012	0.099	1	0.099	0.011	0.366	0.000	6.65	5.34	-39	-29	57
0.012	0.099	1	0.099	0.012	0.380	0.000	6.63	5.33	44	-21	14
0.001	0.032	3	0.008	0.013	0.410	0.000	6.59	5.31	-39	-18	57
0.003	0.063	2	0.025	0.014	0.411	0.000	6.59	5.30	38	36	30
0.001	0.032	3	0.008	0.014	0.425	0.000	6.58	5.29	-39	-15	59
0.012	0.099	1	0.099	0.016	0.457	0.000	6.54	5.28	-5	-75	-30
0.012	0.099	1	0.099	0.016	0.458	0.000	6.54	5.27	-15	30	53
0.012	0.099	1	0.099	0.017	0.483	0.000	6.51	5.26	-12	-3	14
0.003	0.063	2	0.025	0.019	0.523	0.000	6.48	5.24	-36	-57	41
0.003	0.063	2	0.025	0.021	0.558	0.000	6.45	5.22	-53	-45	26
0.012	0.099	1	0.099	0.021	0.558	0.000	6.44	5.22	3	-48	33
0.012	0.099	1	0.099	0.022	0.568	0.000	6.43	5.22	47	-29	53
0.003	0.063	2	0.025	0.023	0.588	0.000	6.42	5.21	-27	-6	57
0.012	0.099	1	0.099	0.024	0.604	0.000	6.40	5.20	-54	-63	12
0.012	0.099	1	0.099	0.025	0.611	0.000	6.40	5.19	0	-69	-21

0.000	0.015	4	0.003	0.026	0.636	0.000	6.38	5.18	12	-29	3
0.012	0.099	1	0.099	0.026	0.645	0.000	6.37	5.18	-12	0	14
0.012	0.099	1	0.099	0.028	0.676	0.000	6.35	5.17	44	-21	53
0.012	0.099	1	0.099	0.029	0.686	0.000	6.35	5.17	-15	26	56
0.012	0.099	1	0.099	0.029	0.690	0.000	6.34	5.16	-41	-33	-12
0.012	0.099	1	0.099	0.031	0.717	0.000	6.32	5.15	-32	-30	9
0.012	0.099	1	0.099	0.035	0.790	0.000	6.28	5.13	2	27	42
0.012	0.099	1	0.099	0.037	0.812	0.000	6.26	5.12	-53	-68	15
0.012	0.099	1	0.099	0.038	0.840	0.000	6.24	5.11	42	36	29
0.012	0.099	1	0.099	0.041	0.870	0.000	6.23	5.10	2	-63	-24
0.012	0.099	1	0.099	0.042	0.885	0.000	6.22	5.10	27	56	18
0.012	0.099	1	0.099	0.043	0.892	0.000	6.22	5.09	-57	-45	26
0.012	0.099	1	0.099	0.046	0.940	0.000	6.19	5.08	-15	33	53
0.012	0.099	1	0.099	0.047	0.956	0.000	6.19	5.07	-36	-32	59
0.012	0.099	1	0.099	0.048	0.976	0.000	6.18	5.07	42	-29	54

Table 10. Display of whole-brain univariate fMRI analysis (paired *t*-test). *Note.* u.c.=uncorrected.

Table 11 Concatenated statistical analysis of ROI

ROI	NAL		CON		*t*	*p*
	M	**SD**	**M**	**SD**		
Nodal Cluster Coefficient						
INS	0.25	0.038	0.28	0.07	-5.9	<.0001
CC	0.26	0.06	0.25	0.05	2.42	<.05
pINS	0.24	0.03	0.27	0.04	-5.26	<.0001
pCC	0.26	0.07	0.25	0.05	3.36	<.0001
mPFC	0.29	0.07	0.23	0.03	5.12	<.0001
Nodal Local Efficiency						
pINS	0.34	0.02	0.35	0.03	-2.92	<.01
Nodal Efficiency						
pINS	0.034	0.03	0.35	0.03	-2.91	<.001

Table 10. Display of region wise statistical analyses (also employed for visualization of probability density plots) for the Nodal cluster coefficient, Nodal Local Efficiency and Nodal Efficiency. A paired t-test (FDR-corrected) was conducted. For the statistical analysis, all subregions corresponding to a region were summarized and subsequently allocated for statistical testing. Only significant regions are displayed. *Note. INS=insula; MINS=medial insula; PINS=posterior insula; CC=cingulate cortex; PCC=posterior cingulate cortex; MPFC=medial prefrontal cortex.*

Table 12 Dosenbach Atlas (Dosenbach, 2010)

Labels	Region	Side	Network	MNI		
				x	y	z
1	vmPFC	R	default	6	64	3
2	mPFC		default	0	51	32
3	aPFC	L	default	-25	51	27
4	vmPFC	R	default	9	51	16
5	vmPFC	L	default	-6	50	-1
6	vmPFC	L	default	-11	45	17
7	vmPFC	R	default	8	42	-5
8	ACC	R	default	9	39	20
9	vlPFC	R	default	46	39	-15
10	sup frontal	R	default	23	33	47
11	sup frontal	L	default	-16	29	54
12	inf temporal	R	default	52	-15	-13
13	inf temporal	L	default	-59	-25	-15
14	post cingulate	R	default	1	-26	31
15	fusiform	R	default	28	-37	-15
16	precuneus	L	default	-3	-38	45
17	post cingulate	L	default	-8	-41	3
18	inf temporal	L	default	-61	-41	-2
19	occipital	L	default	-28	-42	-11
20	post cingulate	L	default	-5	-43	25
21	precuneus	R	default	9	-43	25
22	precuneus	R	default	5	-50	33
23	post cingulate	L	default	-5	-52	17
24	post cingulate	R	default	10	-55	17
25	precuneus	L	default	-6	-56	29
26	post cingulate	L	default	-11	-58	17
27	angular gyrus	R	default	51	-59	34
28	angular gyrus	L	default	-48	-63	35
29	precuneus	R	default	11	-68	42
30	IPS	L	default	-36	-69	40
31	occipital	L	default	-9	-72	41
32	occipital	R	default	45	-72	29
33	occipital	L	default	-2	-75	32
34	occipital	L	default	-42	-76	26
35	aPFC	R	fronto-parietal	29	57	18
36	aPFC	L	fronto-parietal	-29	57	10
37	vent aPFC	R	fronto-parietal	42	48	-3
38	vent aPFC	L	fronto-parietal	-43	47	2
39	vlPFC	R	fronto-parietal	39	42	16
40	dlPFC	R	fronto-parietal	40	36	29
41	ACC	L	fronto-parietal	-1	28	40
42	dlPFC	R	fronto-parietal	46	28	31
43	vPFC	L	fronto-parietal	-52	28	17
44	dlPFC	L	fronto-parietal	-44	27	33
45	dFC	R	fronto-parietal	40	17	40
46	dFC	R	fronto-parietal	44	8	34
47	dFC	L	fronto-parietal	-42	7	36
48	IPL	L	fronto-parietal	-41	-40	42
49	IPL	R	fronto-parietal	54	-44	43
50	post parietal	L	fronto-parietal	-35	-46	48

51	IPL	L	fronto-parietal	-48	-47	49
52	IPL	L	fronto-parietal	-53	-50	39
53	IPL	R	fronto-parietal	44	-52	47
54	IPS	L	fronto-parietal	-32	-58	46
55	IPS	R	fronto-parietal	32	-59	41
56	aPFC	R	cingulo-opercular	27	49	26
57	vPFC	R	cingulo-opercular	34	32	7
58	ACC	L	cingulo-opercular	-2	30	27
59	vFC	R	cingulo-opercular	51	23	8
60	ant insula	R	cingulo-opercular	38	21	-1
61	dACC	R	cingulo-opercular	9	20	34
62	ant insula	L	cingulo-opercular	-36	18	2
63	basal ganglia	L	cingulo-opercular	-6	17	34
64	mFC		cingulo-opercular	0	15	45
65	vFC	L	cingulo-opercular	-46	10	14
66	basal ganglia	L	cingulo-opercular	-20	6	7
67	basal ganglia	R	cingulo-opercular	14	6	7
68	vFC	L	cingulo-opercular	-48	6	1
69	mid insula	R	cingulo-opercular	37	-2	-3
70	thalamus	L	cingulo-opercular	-12	-3	13
71	thalamus	L	cingulo-opercular	-12	-12	6
72	thalamus	R	cingulo-opercular	11	-12	6
73	mid insula	R	cingulo-opercular	32	-12	2
74	mid insula	L	cingulo-opercular	-30	-14	1
75	basal ganglia	R	cingulo-opercular	11	-24	2
76	post insula	L	cingulo-opercular	-30	-28	9
77	temporal	R	cingulo-opercular	51	-30	5
78	post cingulate	L	cingulo-opercular	-4	-31	-4
79	fusiform	R	cingulo-opercular	54	-31	-18
80	precuneus	R	cingulo-opercular	8	-40	50
81	parietal	R	cingulo-opercular	58	-41	20
82	temporal	R	cingulo-opercular	43	-43	8
83	parietal	L	cingulo-opercular	-55	-44	30
84	sup temporal	R	cingulo-opercular	42	-46	21
85	angular gyrus	L	cingulo-opercular	-41	-47	29
86	temporal	L	cingulo-opercular	-59	-47	11
87	TPJ	L	cingulo-opercular	-52	-63	15
88	frontal	R	sensorimotor	58	11	14
89	dFC	R	sensorimotor	60	8	34
90	vFC	L	sensorimotor	-55	7	23
91	pre-SMA	R	sensorimotor	10	5	51
92	vFC	R	sensorimotor	43	1	12
93	SMA		sensorimotor	0	-1	52
94	frontal	R	sensorimotor	53	-3	32
95	precentral gyrus	R	sensorimotor	58	-3	17
96	mid insula	L	sensorimotor	-42	-3	11
97	precentral gyrus	L	sensorimotor	-44	-6	49
98	parietal	L	sensorimotor	-26	-8	54
99	precentral gyrus	R	sensorimotor	46	-8	24
100	precentral gyrus	L	sensorimotor	-54	-9	23
101	precentral gyrus	R	sensorimotor	44	-11	38
102	parietal	L	sensorimotor	-47	-12	36
103	mid insula	R	sensorimotor	33	-12	16
104	mid insula	L	sensorimotor	-36	-12	15

105	temporal	R	sensorimotor	59	-13	8
106	parietal	L	sensorimotor	-38	-15	59
107	parietal	L	sensorimotor	-47	-18	50
108	parietal	R	sensorimotor	46	-20	45
109	parietal	L	sensorimotor	-55	-22	38
110	precentral gyrus	L	sensorimotor	-54	-22	22
111	temporal	L	sensorimotor	-54	-22	9
112	parietal	R	sensorimotor	41	-23	55
113	post insula	R	sensorimotor	42	-24	17
114	parietal	R	sensorimotor	18	-27	62
115	parietal	L	sensorimotor	-38	-27	60
116	parietal	L	sensorimotor	-24	-30	64
117	post parietal	L	sensorimotor	-41	-31	48
118	temporal	L	sensorimotor	-41	-37	16
119	temporal	L	sensorimotor	-53	-37	13
120	sup parietal	R	sensorimotor	34	-39	65
121	occipital	L	occipital	-18	-50	1
122	occipital	L	occipital	-34	-60	-5
123	occipital	R	occipital	36	-60	-8
124	temporal	R	occipital	46	-62	5
125	occipital	L	occipital	-44	-63	-7
126	occipital	R	occipital	19	-66	-1
127	occipital	R	occipital	17	-68	20
128	occipital	R	occipital	39	-71	13
129	occipital	R	occipital	29	-73	29
130	occipital	L	occipital	-29	-75	28
131	occipital	L	occipital	-16	-76	33
132	occipital	R	occipital	9	-76	14
133	occipital	R	occipital	15	-77	32
134	occipital	R	occipital	20	-78	-2
135	post occipital	L	occipital	-5	-80	9
136	post occipital	R	occipital	29	-81	14
137	post occipital	R	occipital	33	-81	-2
138	post occipital	L	occipital	-37	-83	-2
139	post occipital	L	occipital	-29	-88	8
140	post occipital	R	occipital	13	-91	2
141	post occipital	R	occipital	27	-91	2
142	post occipital	L	occipital	-4	-94	12
143	lat cerebellum	L	cerebellum	-28	-44	-25
144	lat cerebellum	L	cerebellum	-24	-54	-21
145	inf cerebellum	L	cerebellum	-37	-54	-37
146	lat cerebellum	L	cerebellum	-34	-57	-24
147	med cerebellum	L	cerebellum	-6	-60	-15
148	inf cerebellum	L	cerebellum	-25	-60	-34
149	inf cerebellum	R	cerebellum	32	-61	-31
150	med cerebellum	L	cerebellum	-16	-64	-21
151	lat cerebellum	R	cerebellum	21	-64	-22
152	med cerebellum	R	cerebellum	1	-66	-24
153	inf cerebellum	L	cerebellum	-34	-67	-29
154	med cerebellum	L	cerebellum	-11	-72	-14
155	inf cerebellum	R	cerebellum	33	-73	-30
156	med cerebellum	R	cerebellum	5	-75	-11
157	med cerebellum	R	cerebellum	14	-75	-21
158	inf cerebellum	L	cerebellum	-21	-79	-33

159	inf cerebellum	L	cerebellum	-6	-79	-33
160	inf cerebellum	R	cerebellum	18	-81	0

Table 12. Display of all regions entailed in the Dosenbach Atlas (Dosenbach et al., 2010)

Table 13 Pearsons correlation between behavioral and graph measures

Nodal Cluster Coefficient (AUC)								
SP	**Region**	**MNI**			**Mean**	**Std**	***R***	***p***
	BG	-20	6	7	0.27	0.04	0.35	<.05
	mINS	32	-12	2	0.19	0.02	0.33	<.05
	PrecGyr	-54	-22	22	0.25	0.09	0.39	<.05
	pINS	42	-24	17	0.23	0.10	0.42	<.01
SNP	dFC	-42	7	36	0.26	0.34	0.36	<.05
	Precuneus	8	-40	50	0.25	0.33	0.42	<.01
	Parietal	-24	-30	64	0.31	0.07	0.40	<.01
	Cerebellum	14	-75	-21	0.19	0.02	0.32	<.05
OP	mPFC	0	51	32	0.26	0.05	0.44	<.01
	vlPFC	39	42	16	0.28	0.07	0.37	<.05
	IPL	54	-44	43	0.23	0.03	0.40	<.01
	Thalamus	11	-12	6	0.20	0.025	0.31	<.05
	Temporal	-54	-22	9	0.26	0.080	0.35	<.05
	Post Occipital	27	-91	2	0.28	0.043	0.31	<.05
ONP	BG	-20	6	7	0.28	0.039	0.42	<.01
	dFC	60	8	34	0.27	0.050	0.33	<.05
	Parietal	-24	-30	64	0.31	0.07	0.32	<.05
	InfCerebellum	-37	-54	-37	0.22	0.027	0.37	<.05
Nodal Efficiency (AUC)								
SP	BG	-20	6	7	0.35	0.035	0.50	<.001
	PrecGyr	-54	-22	22	0.32	0.083	0.44	<.01
	pINS	42	-24	17	0.29	0.11	0.43	<.01
	postOccipital	-5	-80	9	0.31	0.029	0.32	<.05
SNP	Occipital	-9	-72	41	0.26	0.029	0.35	<.05
	dFC	-42	7	36	0.26	0.34	0.37	<.05
	Precuneus	8	-40	50	0.25	0.033	0.40	<.01
	Parietal	-24	-30	64	0.31	0.07	0.35	<.05
	medCerebellum	14	-75	-21	0.19	0.02	0.31	<.05
OP	mPFC	0	51	32	0.34	0.04	0.44	<.01
	vlPFC	39	42	16	0.34	0.06	0.41	<.01
	IPL	54	-44	43	0.33	0.027	0.37	<.05
	Temporal	-54	-22	9	0.33	0.069	0.33	<.05
	Occipital	29	-73	29	0.30	0.027	0.37	<.05
ONP	Occipital	-9	-72	41	0.35	0.020	0.35	<.05
	dFC	-42	7	36	0.35	0.026	0.37	<.05
	Precuneus	8	-40	50	0.34	0.030	0.40	<.01

	Parietal	-24	-30	64	0.37	0.057	0.35	<.05
	MedCerebellum	14	-75	-21	0.31	0.02	0.31	<.05
Nodal Local Efficiency (AUC)								
SP	vmPFC	-6	50	1	0.26	0.031	0.37	<.05
	Occipital	-42	-76	26	0.26	0.027	0.46	<.01
	BG	-20	6	7	0.26	0.021	0.38	<.05
	vFC	-48	6	1	0.025	0.020	0.36	<.05
	PrecGyr	-54	-22	22	0.024	0.057	0.51	<.001
	pINS	42	-24	17	0.023	0.080	0.47	<.01
	postOccipital	-5	-80	9	0.28	0.016	0.31	<.05
SNP	Occipital	45	-72	29	0.27	0.020	0.35	<.05
	Occipital	-42	-76	26	0.26	0.027	0.33	<.05
	aINS	-36	18	2	0.25	0.031	0.31	<.05
	mINS	-42	-3	11	0.26	0.031	0.32	<.05
	Occipital	39	-71	13	0.27	0.011	0.40	<.01
OP	mPFC	0	51	32	0.26	0.022	0.38	<.05
	Occipital	-42	-76	26	0.26	0.027	0.31	<.05
	vFC	-48	6	1	0.25	0.020	0.43	<.01
	Temporal	-54	-22	9	0.25	0.041	0.42	<.01
	Parietal	18	-27	62	0.24	0.029	0.34	<.05
ONP	AG	51	-59	34	0.27	0.016	0.33	<.05
	Occipital	45	-72	29	0.27	0.020	0.37	<.05
	aINS	38	21	-1	0.26	0.026	0.31	<.05
	mINS	-42	-3	11	0.26	0.031	0.36	<.05
	Parietal	-55	-22	38	0.25	0.037	0.32	<.05
	Occipital	17	-68	20	0.27	0.031	0.32	<.05
	Occipital	39	-71	13	0.27	0.011	0.39	<.05
	MedCerebellum	-6	-60	-15	0.27	0.018	0.32	<.05

Table 13. Display of Pearsons correlation between behavioral measures and graph theoretical measures. *Note. SP=Self Pain; SNP=Self No Pain; OP=Other pain; ONP=Other no pain.*